

# Downgoing plate-buoyancy driven retreat of North Sulawesi Trench: transition of a passive margin into a subduction zone

Miao Dong<sup>1</sup>, Tianyao Hao<sup>2</sup>, ChuanChuan Lü<sup>3</sup>, and Jian Zhang<sup>4</sup>

<sup>1</sup>Institute of Geology and Geophysics, Chinese Academy of Sciences

<sup>2</sup>Chinese Academy of Science

<sup>3</sup>University of Cambridge

<sup>4</sup>University of Chinese Academy of Sciences

November 22, 2022

## Abstract

The transition of a passive continental margin into a subduction zone remains a hypothesis because few geological cases have been reported. The North Sulawesi subduction zone is a 5-9 myr system in Southeast Asia that has evolved from a continental passive margin and has long been overlooked by studies of passive to active margin transitions. Here we compare geophysical data from the region with numerical simulation results. We find that the initial subduction of North Sulawesi must rely on horizontal forces, while the trench retreat depends on the negative buoyancy of the oceanic lithosphere. Furthermore, less space available for subduction leads to lower mantle flow caused by subduction and slower trench retreat. These new dynamical constraints indicate that the negative buoyancy of the oceanic plate is the key factor for subduction and trench retreat, even though the subduction initiation was induced.

Downgoing plate-buoyancy driven retreat of North Sulawesi Trench: transition of a passive margin into a subduction zone

Miao Dong<sup>1,2\*</sup>, Tian Yao Hao<sup>1,2\*</sup>, Chuan Chuan Lü<sup>3</sup>, and Jian Zhang<sup>2</sup>

<sup>1</sup>Key Laboratory of Petroleum Resource Research, Institute of Geology and Geophysics, Chinese Academy of Sciences, Beijing 100029, China

<sup>2</sup>University of Chinese Academy of Sciences, Beijing 100049, China

<sup>3</sup>Bullard Labs, Department of Earth Sciences, University of Cambridge, Cambridge CB3 0EZ, UK

Corresponding author: Miao Dong ([dongmiao@mail.iggcas.ac.cn](mailto:dongmiao@mail.iggcas.ac.cn))

Tian Yao Hao ([tyhao@mail.iggcas.ac.cn](mailto:tyhao@mail.iggcas.ac.cn))

## Key Points:

- Subduction initiation of North Sulawesi subduction zone was induced but the trench retreat are driven by the subducted plate itself.
- Subduction-driven mantle flows play an important role in trench motion and upper plate deformation.
- The reason for the clockwise rotation of the North Arm of Sulawesi at present is the presence of the Sangihe slab.

Abstract

The transition of a passive continental margin into a subduction zone remains a hypothesis because few geological cases have been reported. The North Sulawesi subduction zone is a 5–9 myr system in Southeast Asia that has evolved from a continental passive margin and has long been overlooked by studies of passive to active margin transitions. Here we compare geophysical data from the region with numerical simulation results. We find that the initial subduction of North Sulawesi must rely on horizontal forces, while the trench retreat depends on the negative buoyancy of the oceanic lithosphere. Furthermore, less space available for subduction leads to lower mantle flow caused by subduction and slower trench retreat. These new dynamical constraints indicate that the negative buoyancy of the oceanic plate is the key factor for subduction and trench retreat, even though the subduction initiation was induced.

## Plain Language Summary

Transition of a passive margin into a subduction zone is the key process of the Earth. However, our understanding for the dynamic mechanism of this process is still ambiguous. North Sulawesi Trench provides unique opportunities to study it. Since the North Sulawesi Trench is located in an area where the plates converge, its formation and retreat have been thought to have been driven by the collision of the surrounding plates. However, our simulations suggest that the subduction initiation was caused by the compression of other plates, but the trench retreat is a consequence of the negative buoyancy of the subducted plate itself. Mantle convection driven by subducted slab plays an important role in trench retreat and overriding plate deformation. The rotation of North Arm of Sulawesi is also not due to the collision of the surrounding plates, but because the trench retreat more slowly on its eastern side than on its western side. The reason for the different retreating speed is that the subduction space on the east side of the trench is reduced by the Sangihe slab.

## 1 Introduction

In the Wilson cycle theory, the oceanic plate formed by seafloor spreading subducts beneath the continental margin. Numerous young subduction zones were formed during the Cenozoic, but there have been few reports of subduction initiation at passive continental margins (Stern, 2004; Stern and Gerya, 2018). Subduction initiation at passive continental margins remains a very popular hypothesis that is supported by some numerical modelling studies (eg. Marques et al., 2013; Nikolaeva et al., 2010, 2011; Rey et al., 2014; Zhong and Li, 2019). However, in the absence of geological evidence, it remains a subject of constant research and debate (Leng and Gurnis, 2015; Mueller and Phillips, 1991; Stern and Gerya, 2018).

The North Sulawesi Subduction Zone (NSZZ) is located at the convergence of the Sunda, Australia, and Philippine Sea plates and only about 500 km long (Figure 1a). Magnetic anomalies and plate reconstruction indicate that the spreading of the Celebes Sea basin occurred along a north-northwest to south-southeast axis between approximately 48 and 40 Ma (Gaina and Müller, 2007; Hall, 2012; Rangin and Silver, 1991; Weissel, 1980). The southward subduction of the Celebes Sea plate began in approximately 9–5 Ma (Hall, 2012; Lai et al., 2021). The maximum depth of the subducted plate is about 260 km (Figure 1b). It has been overlooked as an excellent location for the study of the transition from passive to active margin (Hall, 2019).

Trench migration is closely correlated with overriding plate deformation and lateral migration of the subducted slab (Funiciello et al., 2008; Holt et al., 2015; Schellart, 2008). The North Sulawesi Trench has retreated since the post-Miocene. Now, the overriding plate–North Arm of Sulawesi is rotating clockwise around its eastern end (Socquet et al., 2006) (Figure 1a). The conventional view is that the collision of the surrounding plates led to the formation of the NSSZ and the retreat of the trench (Kopp et al., 1999; Silver et al., 1983). However, the Sunda plate is moving slowly towards the southeast, while the Australia plate (in the south) and the Philippine Sea plate (in the northeast) are moving rapidly towards the northeast and the northwest, respectively (Figure 1a). If the movement of these three plates was the dominant mechanism underlying the retreat of the North Sulawesi Trench, the North Arm of Sulawesi would have been more prone to counterclockwise. Thus, the trench retreat and rotation mechanism of the North Sulawesi Trench remains unclear.

In this study, we conduct a series of thermomechanical model simulations to investigate the initial subduction

and trench retreat mechanisms of the NSSZ, which is representative of the transition of a passive margin into a subduction zone. Variable boundary conditions are applied, representing different dynamic mechanism. Trench retreat is driven by either overriding plate or subducted plate, which results in different regime diagrams. The model results are compared to the observations in North Sulawesi. The mechanism of model that best fit the observations is the subduction and trench movement mechanism of the NSSZ.

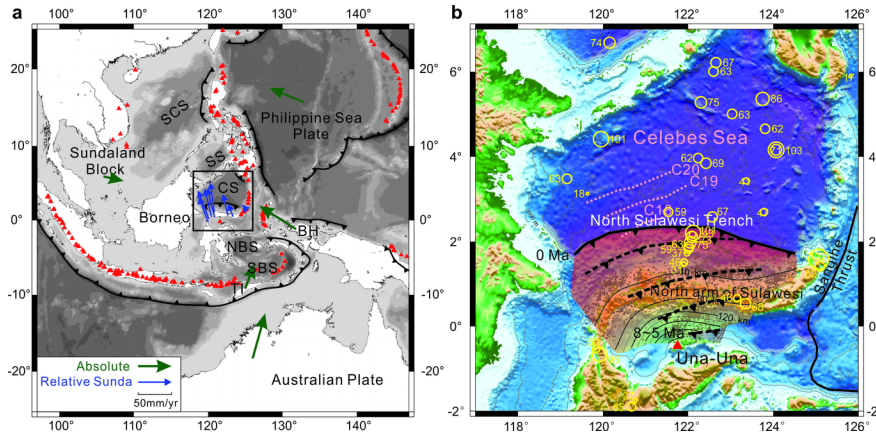


**Figure 1.** Structure-tectonic maps of the Celebes Sea and surrounding area. (a) Location of the study area—Celebes Sea (CS)—within the wider Southeast Asian region, including the Sulu Sea (SS), the South China Sea (SCS), the north Banda Sea (NBS) and the south Banda Sea (SBS). Thick lines indicate subduction zones; triangles on the lines indicate the down-dip direction. Plate motions are indicated by the arrows (Mustafar et al., 2017; Kreemer et al., 2014). Red triangles indicate volcanoes (Global Volcanism Program, 2013). (b) Regional topographic map. The yellow hollow circles are heat flow measurements (Fuchs et al., 2021). The pink dashed lines show the major magnetic anomalies (Weissel, 1980). The irregular shape with transparent colour gradient represents the subducted plate; colours indicate depth. The dotted lines with triangles indicate trench retreat. Events in the EHB catalogue (Engdahl et al., 2020) are represented by black circles.

### Model setup

We used the geodynamic code ASPECT (Advanced Solver for Problems in Earth’s ConvecTion, version 2.3.0-pre) to setup a series of 2D subduction models. The initial model consists of oceanic plate and continental plate on either side (Figure 2a). According to the evolutionary history of NSSZ, the age of oceanic plate is taken to be 40 Ma. The oceanic lithosphere geotherm corresponds to a half-space cooling model for a seafloor age of 40 Ma. The thickness of oceanic plate is therefore set to 82 km. The oceanic crust consists of two layers and is 10 km thick in total. The composition for the mantle part of the oceanic lithosphere and for the asthenosphere are taken to be identical. The density of them is both set to  $3300 \text{ kg/m}^3$ . The continental plate consists of upper crust, lower crust and lithospheric mantle. The continental crust is set to 30 km based on the current crustal thickness of Sulawesi (Fauzi et al., 2021). Because the initial lithospheric thickness, density of lithospheric mantle and ocean-continent transition angle have never been definitely settled, we vary the values of these three parameters to investigate their effect on the spontaneous subduction (Table 1). Temperature structure of the continental plate is controlled by the lithospheric thickness and is defined by a steady state profile from 0 at the surface to 1300 at the base of lithosphere (Figure 2a).

Spontaneous and induced subductions are modelled by controlling the boundary conditions and density differences between oceanic plate and asthenosphere. The spontaneous models (Experiment 1~24) have all free slip boundaries (Figure 2a) and the Gabbro-Eclogite phase transition for the oceanic crust was implemented. Density of oceanic crust increases from  $3000 \text{ kg/m}^3$  to  $3450 \text{ kg/m}^3$  at pressures of  $\sim 1.9 \text{ GPa}$  ( $\sim 60 \text{ km}$  depth). In the induced model (Experiment 25~30), horizontal far field forces are represented by

specifying a convergence velocity ( $V_{in}$ ) on one side of the overriding plate; the Gabbro-Eclogite phase transition for the oceanic crust was not executed.

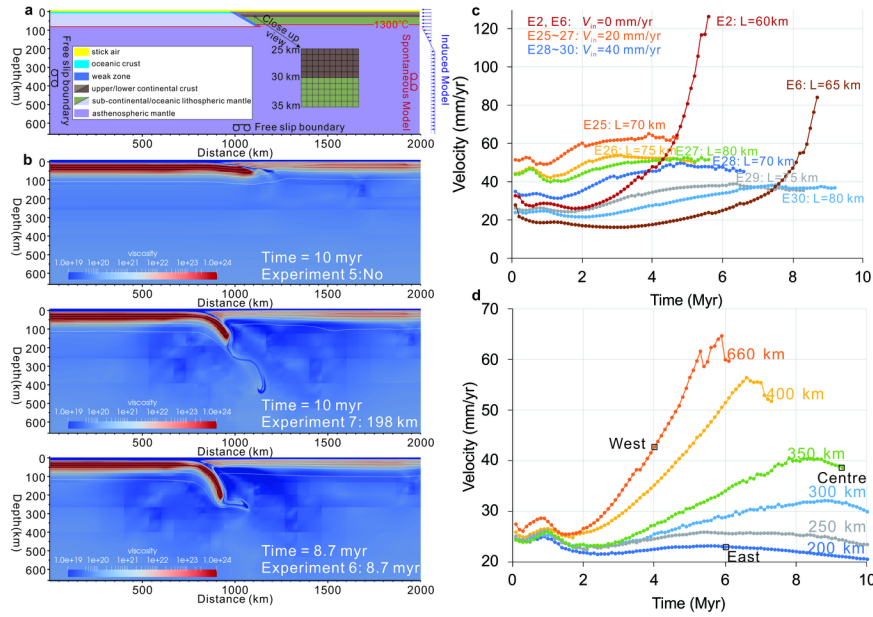


**Figure 2.** Initial model and modeling results. (a) Initial model setup with model geometry, layer characteristics, and thermal configuration. (b) Three cases show different results: no subduction (Experiment 5); subducted slab did not reach a depth of 260 km within 10 myr (Experiment 7); subduction depth of 260 km within 10 myr (Experiment 6). (c) Variation of trench retreat velocities with time for experiments with different mechanism (Density of continental lithospheric mantle =  $3275 \text{ kg/m}^3$ ; Ocean-continent transition angle =  $30^\circ$ ). (d) Trench retreat velocity of the coupled model with depth 660 km, 400 km, 350 km, 300 km, 250 km, 200km. West, Centre, East indicate the trench retreat velocity on the western side, centre and eastern side of Celebes Sea, respectively.

**Table 1.** Parameters and Descriptions of Numerical Experiments

Experiment	$V_{in}$ (mm/yr)	Thickness of continental plate (km)	Density of Continental lithospheric mantle ( $\text{kg/m}^3$ )	C
1	0	60	3275	1
2	0	60	3275	3
3	0	60	3275	4
4	0	60	3275	6
5	0	65	3275	1
6	0	65	3275	3
7	0	65	3275	4
8	0	65	3275	6
9	0	70	3275	1
10	0	70	3275	3
11	0	70	3275	4
12	0	70	3275	6
13	0	60	3250	1
14	0	60	3250	3
15	0	60	3250	4
16	0	60	3250	6

Experiment	$V_{in}$ (mm/yr)	Thickness of continental plate (km)	Density of Continental lithospheric mantle ( $\text{kg/m}^3$ )	C
17	0	65	3250	1
18	0	65	3250	3
19	0	65	3250	4
20	0	65	3250	6
21	0	70	3250	1
22	0	70	3250	3
23	0	70	3250	4
24	0	70	3250	6
25	40	70	3275	3
26	40	75	3275	3
27	40	80	3275	3
28	20	70	3275	3
29	20	75	3275	3
30	20	80	3275	3
31	20	75	3275	3
32	20	75	3275	3
33	20	75	3275	3
34	20	75	3275	3
35	20	75	3275	3
36	20	75	3275	3

### 3 Model Results

#### 3.1 Parameters that affect spontaneous subduction

Since the subduction initiation of NSSZ occurred at 5–9 Ma and the maximum depth of the subducted slab is about 260 km at present. The simulation ends when the subducted slab reaches a depth of 260 km or the time reaches 10 myr. If the oceanic slab does not exceed a depth of 150 km within 10 myr, we denote it by “No” (Figure 2b and Table 1). If the maximum depth of the subducted slab is deeper than 150 km but shallower than 260 km (Figure 2b), we list the depth. For the experiments where the slab reached 260 km depth within 10 myr, we list this time (Figure 2b).

Experiments show transition from fast to slow subduction with increasing thickness of the continental lithosphere. Spontaneous subduction initiation is almost impossible to occur with 70 km or more thick continental plate (Experiment 9–12, 21–24). The effect of density contrast is opposite to that of the thickness of the continental plate. A larger density contrast promotes spontaneous subduction initiation. The ocean-continent boundary angle has a nonlinear effect on the spontaneous subduction initiation. Either too large ( $60^\circ$ ) or too small ( $15^\circ$ ) angle are all adverse to spontaneous subduction initiation. The thickness and density of the continental lithospheric mantle and the ocean-continent boundary angle all affect whether subduction initiation occurs spontaneously. It suggests that the force due to the density difference between the continental and oceanic plate is the main force leading to the spontaneous subduction initiation.

#### 3.2 Trench retreat velocity in spontaneous and induced model experiments

Trench location and speed are inferred from the location and speed of the edge of the continental crust that is the farthest forward in the model. In all spontaneous and induced model experiments, trench retreat speed increases and then decreases during the first 1–2 myr (Figure 2c). At the beginning of the simulation period, the density difference between the continental and oceanic crusts gives rise to lateral stresses that push the continental crust towards the ocean; as the difference between the stresses decreases, trench retreat speed decreases gradually. This process is active in approximately 2 myr.

After the first 2 myr in the spontaneous model (Figure 2c), subduction depth increases, the trench retreat velocity increases correspondingly. The increasing begins slowly, then more and more rapidly. It is because as the oceanic plate sinks, there are more and more eclogite-face oceanic crust to increase the negative buoyancy of the subducted slab. In the induced model, the trench retreat speed increasing slowly, then becoming almost constant. The final speed is slightly greater than the specified velocity  $V_{in}$ .

### 3.3 Deformation and heat flow of the overriding plate

The deformation of the overriding plate varies in the different subduction models. In the spontaneous subduction model, the rollback of the subducted plate obviously causes stretching of the overriding plate. The crustal thickness decreased from 30 km to about 23 km (eg. Experiment 2, 3). In the induced subduction model, the overriding plate thrusts over the subducted plate, and the overriding plate is slightly thinned (Experiment 25–30). The latest published geological profile of the North Arm of Sulawesi indicates lithospheric significant extension between the Late Miocene and Pliocene (Nugraha et al., 2022, Advokaat et al., 2017), which is consistent with the results of the spontaneous subduction model.

The heat flow of the overriding plate is closely related to the lithospheric thickness either in spontaneous or induced model experiments. It is opposite to the continental lithospheric thickness. The values of heat flow listed in Table 1 is the calculated surface heat flow which lies at a distance of 100 km above the top of the subducted slab. It corresponds to the location of the maximum heat flow (68 mW/m<sup>2</sup>) on the North Arm of Sulawesi (Figure 1b). In all the experiments, the model with 75 km thick continental lithosphere has the closest value to that observation. The heat flow values in models have a 70 km or thinner lithosphere are all greater than the maximum observed values.

## 4 Discussion

### 4.1 Implications for transition of passive margins into subduction zones

The mechanism of subduction initiation at passive margins have been studied by several numerical simulations (Faccenna et al., 1999; Goren et al., 2008; Marques et al., 2014; Turcotte et al., 1977; Zhou et al., 2020). Our intention is not repeat other studies and prove the feasibility of spontaneous subduction initiation at passive margins, but to estimate the subduction mechanism through the constraints of the geological case–NSSZ. The spontaneous and induced subduction models represent the extreme cases of subduction driven by horizontal far-field forces and of subduction driven by the negative buoyancy of the down-going plate itself. Examples of completely spontaneous or induced mechanisms are difficult to reproduce the evolution of NSSZ—subduction depth of 260 km after approximately 5–9 myr, 68 mW/m<sup>2</sup> heat flow of the overriding plate and obvious extended continental crust. Because the mainly force that cause the oceanic plate to bend and sink in spontaneous subduction initiation is lateral stress, which is caused by the density difference between the continental plate and the oceanic plate (Nikolaeva et al., 2010). A thick crust and hot lithosphere are necessary to produce the sufficiently large lateral stress (Nikolaeva et al., 2010). According to the present crustal structure and heat flow of North Arm of Sulawesi, spontaneous subduction initiation is unlikely to occur in the NSSZ. Therefore, an external force is necessary to push the continental plate towards the oceanic plate in the early stage of subduction initiation. For the NSSZ, the external force may originate mainly from the collision of the surrounding plates. Because since the Cenozoic, Sulawesi has been at the center of the convergence of surrounding plates (Hall, 2012). This induced mechanism dominates the early stage of subduction initiation, which takes about 2 myr. Once the oceanic crust reaches the depths of ~60 km where eclogite transformation can occur, the main force controlling the subduction begin to change from the horizontal external force to the vertical negative buoyancy of the subducted slab. The subsequent subduction, trench retreat and extension of continental crust are all mainly depend on the negative buoyancy of the subducted slab, as exhibitions in spontaneous model experiments (Table1 and Figure 2). In addition, adjacent areas in the same tectonic setting can also provide insight into the subduction process.

The Sula Deep, Tolo Trough and Cotobato Trench located near the North Sulawesi Trench (Figure 3a, d) are considered to examples of three stages in the subduction initiation. Sula Deep and Tolo Trough is suggested to record the earliest stages and second stage in subduction development, respectively (Hall, 2019). Cotobato

Trench is interpreted as the third stage where a seismically defined slab can be recognized (Hall, 2019). The North Sulawesi Trench represents the final stage, which indicates that subduction initiation is end and a mature subduction zone has been formed. From the topography of these trenches (Figure 3), we can see that each trench has a different landward slope. The areas (Sula Deep and Tolo Trough) in early stage of subduction initiation, has a very steep landward slope (Figure 3b, c). As the subduction development (Cotobato Trench and North Sulawesi Trench), the landward slope changes from steep to gentle (Figure 3e, f).

There are obvious differences in landward slope angles vary in different mechanisms models. In the spontaneous numerical model, the slope gradually smooth with the subduction development (Figure 3g). While the slope in induced model is steeper than that in spontaneous model and the slope can be maintained at a steeper state under the push of far field forces (Figure 3h). Combining the steeper slope in the Sula Deep and Tolo Trough and gentle slope in Cotobato Trench and North Sulawesi Trench, we could also suggest the subduction slab controlled the retreat of the trench.

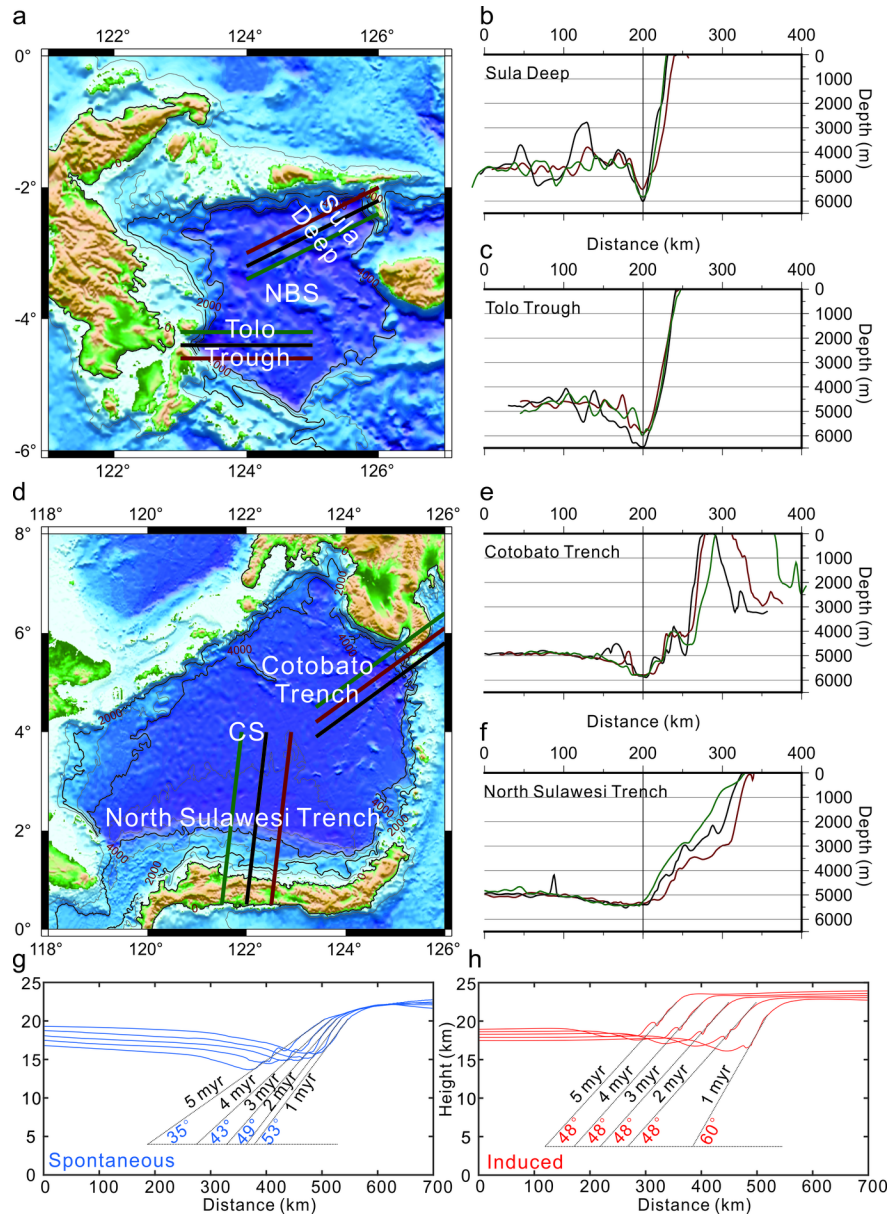


**Figure 3** . The topography profiles of the Sula Deep (b), Tolo Trough (c), Cotobato Trench (e), and North Sulawesi trench (f) and the topographic results simulated by the spontaneous model (g) and induced model (h). Location of Celebes Sea (CS) and north Banda Sea (NBS) are shown in Figure 1a. The black vertical lines at 200 km in (b), (c), (e), (f) indicate the trench location. We put the deepest position of every topography profiles at this location. Because the proportion of horizontal axis and vertical axis is not practical, the angles in the figures (g) and (h) are only used to compare with each other, not the true angles.

#### 4.2 Rotation of the North Arm of Sulawesi

The clockwise rotation of the North Arm of Sulawesi is also consistent with the spontaneous retreat of the North Sulawesi Trench. The negative buoyancy drags the slab down and promotes mantle flow, which determines trench retreat and deformation of the overriding plate (Alsaif et al., 2020). Seismic tomography shows that the Sangihe slab is subducting westward below the Celebes Sea plate (Hall and Spakman, 2015;

Hayes et al., 2018). The subduction depth of the Sangihe slab increases from east to west; hence, the distance between the Celebes Sea plate and the Sangihe slab decreases from west to east, and the two plates are in contact on the eastern side of the Celebes Sea plate (Figure S1). Therefore, the Sangihe slab substantially reduces the space that is available for subduction on the eastern side of the Celebes Sea plate.

This is a complex 3-D situation, we can first simplify it to a two-dimensional model to simulate it. If we cut a section along the north-south direction (Figure S1). The Sangihe slab will be shown as a rectangular block below Celebes Sea on the profile. The distance between the top of the Sangihe slab and the earth's surface on the west side is larger than that on the east side. So we can take the top of the Sangihe slab as the bottom of the model to build simplified models. We conduct experiments using the spontaneous subduction model; model depth is reduced from 660km to 400 km, 350 km, 300 km, 250 km and 200 km, respectively, while parameters and boundary conditions are held constant. We find that the reduction of the space available for subduction leads to the decrease of mantle convection velocity, which in turn reduces the trench retreat velocity (Figure 2d). These results are consistent with the hypothesis that the Sangihe slab reduces the space that is available for subduction, inhibiting spontaneous subduction and slowing down trench retreat on the eastern side (at about 123.5°E) of the Celebes Sea ("East" in Figure 2d). Although the length of the subducted slab is larger on the centre (at about 122°E) than the western side (at about 120.5°E) of Celebes Sea, there is always plenty of space for subduction on the western side of the Celebes Sea. As marked by "West" in Figure 2d, the slab reached to a depth of 150 km and the trench retreat speed increased to ~43 mm/yr during a short time. By contrast, space for subduction on the centre is always limited. As marked by "Centre" in Figure 2d, the trench retreat speed is only ~37 mm/yr, although its subducted slab has reached a depth of 260 km. Hence, trench retreat speed decreases from the western side to the eastern side of the Celebes Sea, resulting in the clockwise rotation of the North Arm of Sulawesi.

However, the 2D models ignored the effect of toroidal flow around the slab edge. Hence, we build a 3D model to simulate this complex natural 3D system (Figure 4). The 3D model consists of a continental plate as overriding plate and two oceanic subducted plates. The subduction direction of the two subduction plates is orthogonal. Model parameters and rheology are same with the 2D model. As we can see from the simulation result (Figure 4), the trench retreat speed simulated by 3D model is also roughly equal to the velocity of the North Arm of Sulawesi measured by GPS. According to the modelling results, we found that the subduction-driven mantle wedge flow is much faster than the toroidal flow around the slab edge. The mantle wedge flow of Sangihe slab is mainly parallel to the North Sulawesi Trench which has little effect on the subduction of Celebes Sea slab. The most important factor that affecting the subduct rate of Celebes Sea slab is also the available space for subduction. Therefore, we proposed that the reason for the clockwise rotation of the North Arm of Sulawesi at present is the presence of the Sangihe slab.

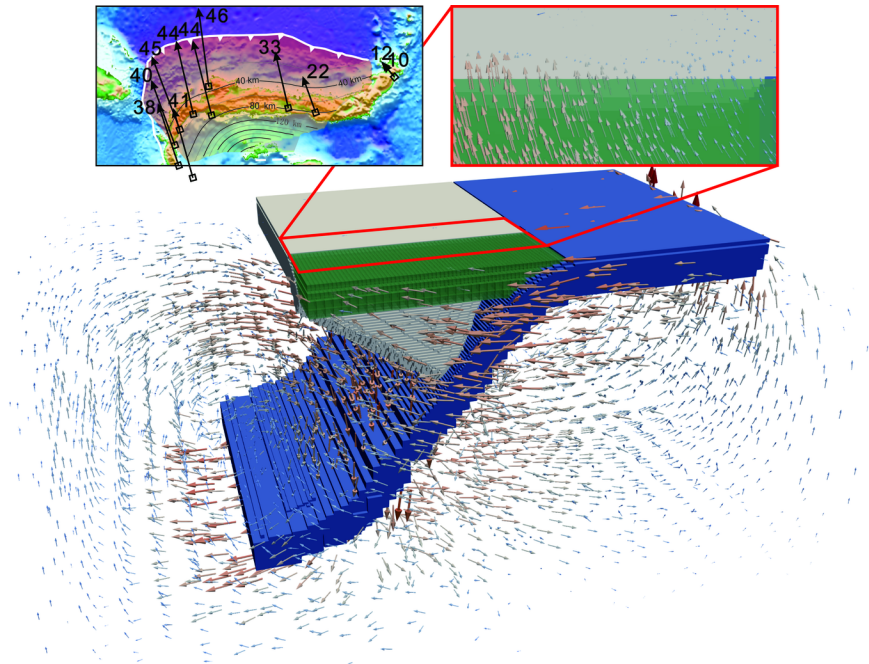


**Figure 4 .** 3D Schematic model (view to the northwest) of the North Sulawesi Subduction Zone. The gray plate represents the Celebes Sea plate. The blue slab represents the Sangihe slab. Arrows indicate velocity. GPS velocities of North Arm of Sulawesi are from Socquet et al. (2006)

## 5 Conclusions

The main conclusions we may draw from this study include the following:

1. Our numerical experiments demonstrate the crucial role that the buoyancy of the down-going plate itself plays in trench retreat as a passive margin transitions into an active margin, even though the initial stage is dominated by the external force.
2. The Sangihe slab reduces the space that is available for subduction, inhibiting spontaneous subduction and slowing down trench retreat on the eastern side of the Celebes Sea, which well explains the clockwise rotation of the North Arm of Sulawesi.

## Acknowledgments

M. D., T. Y. H., and J. Z. acknowledge financial support from the National Natural Science Foundation of China (91858212, 41906056, and 42076068) and the International Partnership Program of the Bureau of International Cooperation of the Chinese Academy of Sciences (132A11KYSB20180020). CC. L. was supported by the Isaac Newton Trust in Cambridge and GCRF (G102642). The authors also thank the Computational Infrastructure for Geodynamics (geodynamics.org), which is funded by the NSF under awards EAR-0949446 and EAR-1550901, for supporting the development of ASPECT.

## Data Availability Statement

The version of ASPECT is available at <https://doi.org/10.5281/zenodo.5131909>. All data that this numerical study is based on can be found in Table S1.

## References

Advokaat, E. L., Hall, R., White, L. T., Watkinson, I. M., Rudyawan, A., & BouDagher-Fadel, M. K. (2017). Miocene to recent extension in NW Sulawesi, Indonesia, *Journal of Asian Earth Sciences*, 147, 1–12.

378-401.<https://doi.org/10.1016/j.jseaes.2017.07.023>

Alsaif, M., F. Garel, F. Gueydan, & D. R. Davies (2020). Upper plate deformation and trench retreat modulated by subduction-driven shallow asthenospheric flows. *Earth and Planetary Science Letters* ,532 ,<https://doi.org/10.1016/j.epsl.2019.116013>

Bangerth, W., Dannberg, J., Gassmoeller, R., & Heister, T. 2020. ASPECT v2.2.0. (version v2.2.0). Zenodo.<https://doi.org/10.5281/ZENODO.3924604>

Engdahl, E. R., Di Giacomo, D., Sakarya, B., Gkarlaouni, C. G., Harris, J., & Storchak, D. A. (2020). ISC-EHB1964-2016, an improved data set for studies of Earth structure and global seismicity. *Earth and Space Science* , 7 , e2019EA000897.<https://doi.org/10.1029/2019EA000897>

Faccenna, C., Giardini, D., Davy, P., & Argentieri, A. (1999). Initiation of subduction at Atlantic-type margins: Insights from laboratory experiments. *Journal of Geophysical Research* ,104 , 2749-2766.<https://doi.org/10.1029/1998JB900072>

Fauzi M. F., Anggraini, A., Riyanto, A., Ngadmanto, D., Suryanto, W., 2021. Crustal thickness estimation in Indonesia using receiver function method, IOP Conf. Series: Earth and Environmental Science 873 (2021) 012086.<https://doi.org/10.1088/1755-1315/873/1/012086>.

Fuchs, Sven; Norden, Ben; International Heat Flow Commission (2021): The Global Heat Flow Database: Release 2021. GFZ Data Services.<https://doi.org/10.5880/figeo.2021.014>

Funiciello, F., C. Faccenna, A. Heuret, S. Lallemand, E. Di Giuseppe, & T. W. Becker (2008). Trench migration, net rotation and slab–mantle coupling. *Earth and Planetary Science Letters* , 271 (1-4), 233-240.<https://doi.org/doi:10.1016/j.epsl.2008.04.006>

Gaina, C., & Müller, D. (2007). Cenozoic tectonic and depth/age evolution of the Indonesian gateway and associated back-arc basins, *Earth-Science Reviews* , 83 (3-4), 177-203.<https://doi.org/10.1016/j.earscirev.2007.04.004>

Glerum, A., Thieulot, C., Fraters, M., Blom, C., & Spakman, W. (2018). Nonlinear viscoplasticity in ASPECT: benchmarking and applications to subduction, *Solid Earth* ,9 (2), 267-294.<https://doi.org/10.5194/se-9-267-2018>

Global Volcanism Program, 2013. Volcanoes of the World, v. 4.9.4 (17 Mar 2021). Venzke, E (ed.). Smithsonian Institution. Downloaded 23 Apr 2021.<https://doi.org/10.5479/si.GVP.VOTW4-2013>.

Goren, L., Aharonov, E., Mulugeta, G., Koyi, H. A., & Mart, Y. (2008). Ductile deformation of passive margins: A new mechanism for subduction initiation, *Journal of Geophysical Research: Solid Earth* ,113 (B8). <https://doi.org/10.1029/2005jb004179>

Hall, C. E., Gurnis, M., Sdrolias, M., Lavier, L. L., Müller, R. D. (2003). Catastrophic initiation of subduction following forced convergence across fracture zones. *Earth and Planetary Science Letters* , 212, 15-30.[https://doi.org/10.1016/S0012-821X\(03\)00242-5](https://doi.org/10.1016/S0012-821X(03)00242-5)

Hall, R. & Spakman, W. (2015). Mantle structure and tectonic history of SE Asia. *Tectonophysics* 658, 14-45.<https://doi.org/10.1016/j.tecto.2015.07.003>

Hall, R. (2012). Late Jurassic–Cenozoic reconstructions of the Indonesian region and the Indian Ocean, *Tectonophysics* ,570-571 , 1-41.<https://doi.org/10.1016/j.tecto.2012.04.021>

Hall, R. (2019). The subduction initiation stage of the Wilson cycle, *Geological Society , London , Special Publications* ,470 (1), 415-437.<https://doi.org/10.1144/SP470.3>

Hayes, G. P., Moore, G. L., Portner, D. E., Hearne, M., Flamme, H., Furtney, M., & Smoczyk, G. M. (2018). Slab2, a comprehensive subduction zone geometry model, *Science* , 362 (6410), 58-61.<https://doi.org/10.1126/science.aat4723>

- Heister, T., Dannberg, J., Gassmüller, R., & Bangerth, W. (2017). High Accuracy Mantle Convection Simulation through Modern Numerical Methods-II: Realistic Models and Problem. *Geophysical Journal International* , 210 , 833-851.<https://doi.org/10.1093/gji/ggx195>
- Hirth, G. & Kohlstedt, D. Rheology of the upper mantle and the mantle wedge: a view from the experimentalists. in *Inside the Subduction Factory* (ed. Eiler, J.) Vol. 183 of *Geophysical Monograph* (American Geophysical Union, 2003).
- Holt, A. F., Becker, T. W., & Buffett, B. A. (2015). Trench migration and overriding plate stress in dynamic subduction models. *Geophysical Journal International* , 201 , 172-192.<https://doi.org/10.1093/gji/ggv011>
- Hu, J., & Gurnis, M. (2020). Subduction Duration and Slab Dip. *Geochemistry, Geophysics, Geosystems* , 21 , e2019GC008862.<https://doi.org/10.1029/2019GC008862>
- Kopp, C., Flueh, E. R., & Neben, S. (1999). Rupture and accretion of the Celebes Sea crust related to the North Sulawesi subduction combined interpretation of reflection and refraction seismic measurements. *Journal of Geodynamics* , 27 (3), 309-325.[https://doi.org/10.1016/S0264-3707\(98\)00004-0](https://doi.org/10.1016/S0264-3707(98)00004-0)
- Kreemer, C., Blewitt, G., & Klein, E. C. (2014). A geodetic plate motion and Global Strain Rate Model. *Geochemistry, Geophysics, Geosystems* , 15 , 3849-3889.<https://doi.org/10.1002/2014GC005407>
- Kronbichler, M., Heister, T., & Bangerth, W. (2012). High Accuracy Mantle Convection Simulation through Modern Numerical Methods. *Geophysical Journal International* , 191 , 12-29.<https://doi.org/10.1111/j.1365-246X.2012.05609.x>
- Lai, C.-K., Xia, X.-P., Hall, R., Meffre, S., Tsikouras, B., Rosana Balangué-Tarriela, M. I., et al. (2021). Cenozoic evolution of the Sulu Sea arc-basin system: An overview. *Tectonics* , 40 , e2020TC006630.<https://doi.org/10.1029/2020TC006630>
- Lallemand, S., Heuret, A., & Boutelier, D. (2005). On the relationships between slab dip, back-arc stress, upper plate absolute motion, and crustal nature in subduction zones. *Geochemistry, Geophysics, Geosystems* , 6 , Q09006.<https://doi.org/10.1029/2005GC000917>
- Leng, W., & Gurnis, M. (2015). Subduction initiation at relic arcs. *Geophysical Research Letters* , 42 (17), 7014-7021.<https://doi.org/10.1002/2015gl064985>
- Marques, F. O., Nikolaeva, K., Assumpção, M., Gerya, T. V., Bezerra, F. H. R., do Nascimento, A. F., & Ferreira, J. M. (2013). Testing the influence of far-field topographic forcing on subduction initiation at a passive margin. *Tectonophysics* , 608 , 517-524.<https://doi.org/10.1016/j.tecto.2013.08.035>
- Marques, F. O., Cabral, F. R., Gerya, T. V., Zhu, G. & May, D. A. (2014). Subduction initiates at straight passive margins. *Geology* , 42 , 331-334.<https://doi.org/10.1130/G35246.1>
- Mueller, S., & Phillips, R. J. (1991). On The initiation of subduction, *Journal of Geophysical Research* , 96 (B1), 651-665.<https://doi.org/10.1029/90jb02237>
- Mustafar, M. A., Simons, W. J. F., Tongkul, F., Satirapod, C., Omar, K. M., & Visser, P. N. A. M. (2017). Quantifying deformation in North Borneo with GPS. *Journal of Geodesy* , 91 , 1241-1259.<https://doi.org/10.1007/s00190-017-1024-z>
- Nikolaeva, K., Gerya, T. V., Marques, F. O. (2010). Subduction initiation at passive margins: Numerical modeling. *Journal of Geophysical Research* , 115 , B03406.<https://doi.org/10.1029/2009JB006549>
- Nikolaeva, K., Gerya, T. V., Marques, F. O. (2011). Numerical analysis of subduction initiation risk along the Atlantic American passive margins. *Geology* 39 , 463-466.<https://doi.org/10.1130/G31972.1>
- Nugraha, A. M. S., Hall, R., & Bou-Dagher-Fadel, M. (2022). The Celebes Molasse: A revised Neogene stratigraphy for Sulawesi, Indonesia. *Journal of Asian Earth Sciences* , 228, 105140.<https://doi.org/10.1016/j.jseaes.2022.105140>

- Rangin, C., & Silver, E. A. (1991). Neogene tectonic evolution of the Celebes-Sulu basins: new insights from leg 124 drilling. *Proceeding of the Ocean Drilling Program, Scientific Result* , 124 , 51-63.
- Rey, P., Coltice, N. & Flament, N. (2014). Spreading continents kick-started plate tectonics. *Nature* , 513 , 405–408. <https://doi.org/10.1038/nature13728>
- Rutter, E. H. & Brodie, K. H. (2004). Experimental grain size-sensitive flow of hotpressed Brazilian quartz aggregates. *Journal of Structural Geology*, 26 , 2011–2023. <https://doi.org/10.1016/j.jsg.2004.04.006>
- Rybacki, E., Gottschalk, M., Wirth, R. & Dresen, G. (2006). Influence of water fugacity and activation volume on the flow properties of fine-grained anorthite aggregates. *Journal of Geophysical Research: Solid Earth* , 111 , 3663. <https://doi.org/10.1029/2005JB003663>
- Schellart, W. P. (2008), Subduction zone trench migration: Slab driven or overriding-plate-driven? *Physics of the Earth and Planetary Interiors* , 170 (1-2), 73-88, <https://doi.org/10.1016/j.pepi.2008.07.040>
- Sharples, W., Jadamec, M. A., Moresi, L. N., & Capitanio, F. A. (2014). Overriding plate controls on subduction evolution, *Journal of Geophysical Research: Solid Earth* , 119 (8), 6684-6704. <https://doi.org/10.1002/2014jb011163>
- Silver, E. A., McCaffrey, R., & Smith, R. B. (1983). Collision, Rotation, and the Initiation of Subduction in the Evolution of Sulawesi, Indonesia. *Journal of Geophysical Research* , 88 , 9407-9418. <https://doi.org/10.1029/JB088iB11p09407>
- Socquet, A., Simons, W., Vigny, C., McCaffrey, R., Subarya, C., Sarsito, D., et al. (2006). Microblock rotations and fault coupling in SE Asia triple junction (Sulawesi, Indonesia) from GPS and earthquake slip vector data, *Journal of Geophysical Research* , 111 (B8). <https://doi.org/10.1029/2005jb003963>
- Stern, R. J. (2004). Subduction initiation: spontaneous and induced, *Earth and Planetary Science Letters* , 226 (3-4), 275-292. [https://doi.org/10.1016/s0012-821x\(04\)00498-4](https://doi.org/10.1016/s0012-821x(04)00498-4)
- Stern, R. J., & Gerya, T. (2018). Subduction initiation in nature and models: A review, *Tectonophysics* , 746 , 173-198. <https://doi.org/10.1016/j.tecto.2017.10.014>
- Turcotte, D. L., Ahern, J. L. & Bird, J. M. (1977). The state of stress at continental margins. *Tectonophysics*, 42 , 1-28. [https://doi.org/10.1016/0040-1951\(77\)90014-2](https://doi.org/10.1016/0040-1951(77)90014-2)
- Turcotte, D. L., & Schubert, G. (2014). *Geodynamics*. Cambridge, UK: Cambridge University Press.
- Weissel, J.K. 1980. Evidence for Eocene oceanic crust in the Celebes Basin. In: Hayes, D.E. (Ed.), *The Tectonic and Geologic Evolution of Southeast Asian Seas and Islands*. American Geophysical Union, Geophysical Monograph Series, 23, 37-47.
- Zhang, J., Hao, T., Dong, M., Xu, Y., Wang, B., Ai, Y., & Fang, G. (2021). Investigation of geothermal structure of the Sulawesi, using gravity and magnetic method. *Science China Earth Sciences* , 64 , 278-293. <https://doi.org/10.1007/s11430-020-9659-3>
- Zhong, X., & Li, Z. H. (2019). Forced Subduction Initiation at Passive Continental Margins: Velocity-Driven Versus Stress-Driven, *Geophysical Research Letters* , 46 (20), 11054-11064. <https://doi.org/10.1029/2019gl084022>
- Zhou, X., Li, Z. H., Gerya, T. V. & Stern, R. J. (2020). Lateral propagation-induced subduction initiation at passive continental margins controlled by preexisting lithospheric weakness. *Science Advances* , 6 , eaaz1048. <https://doi.org/10.1126/sciadv.aaz1048>

Miao Dong<sup>1,2\*</sup>, Tian Yao Hao<sup>1,2\*</sup>, Chuan Chuan Lü<sup>3</sup>, and Jian Zhang<sup>2</sup>

<sup>1</sup>Key Laboratory of Petroleum Resource Research, Institute of Geology and Geophysics, Chinese Academy of Sciences, Beijing 100029, China

<sup>2</sup>University of Chinese Academy of Sciences, Beijing 100049, China

<sup>3</sup>Bullard Labs, Department of Earth Sciences, University of Cambridge, Cambridge CB3 0EZ, UK

Corresponding author: Miao Dong (dongmiao@mail.iggcas.ac.cn)

Tian Yao Hao (tyhao@mail.iggcas.ac.cn)

Key Points:

- Subduction initiation of North Sulawesi subduction zone was induced but the trench retreat are driven by the subducted plate itself.
- Subduction-driven mantle flows play an important role in trench motion and upper plate deformation.
- The reason for the clockwise rotation of the North Arm of Sulawesi at present is the presence of the Sangihe slab.

Abstract

The transition of a passive continental margin into a subduction zone remains a hypothesis because few geological cases have been reported. The North Sulawesi subduction zone is a 5-9 myr system in Southeast Asia that has evolved from a continental passive margin and has long been overlooked by studies of passive to active margin transitions. Here we compare geophysical data from the region with numerical simulation results. We find that the initial subduction of North Sulawesi must rely on horizontal forces, while the trench retreat depends on the negative buoyancy of the oceanic lithosphere. Furthermore, less space available for subduction leads to lower mantle flow caused by subduction and slower trench retreat. These new dynamical constraints indicate that the negative buoyancy of the oceanic plate is the key factor for subduction and trench retreat, even though the subduction initiation was induced.

### Plain Language Summary

Transition of a passive margin into a subduction zone is the key process of the Earth. However, our understanding for the dynamic mechanism of this process is still ambiguous. North Sulawesi Trench provides unique opportunities to study it. Since the North Sulawesi Trench is located in an area where the plates converge, its formation and retreat have been thought to have been driven by the collision of the surrounding plates. However, our simulations suggest that the subduction initiation was caused by the compression of other plates, but the trench retreat is a consequence of the negative buoyancy of the subducted plate itself. Mantle convection driven by subducted slab plays an important role in trench retreat and overriding plate deformation. The rotation of North Arm of

Sulawesi is also not due to the collision of the surrounding plates, but because the trench retreat more slowly on its eastern side than on its western side. The reason for the different retreating speed is that the subduction space on the east side of the trench is reduced by the Sangihe slab.

## 1 Introduction

In the Wilson cycle theory, the oceanic plate formed by seafloor spreading subducts beneath the continental margin. Numerous young subduction zones were formed during the Cenozoic, but there have been few reports of subduction initiation at passive continental margins (Stern, 2004; Stern and Gerya, 2018). Subduction initiation at passive continental margins remains a very popular hypothesis that is supported by some numerical modelling studies (eg. Marques et al., 2013; Nikolaeva et al., 2010, 2011; Rey et al., 2014; Zhong and Li, 2019). However, in the absence of geological evidence, it remains a subject of constant research and debate (Leng and Gurnis, 2015; Mueller and Phillips, 1991; Stern and Gerya, 2018).

The North Sulawesi Subduction Zone (NSSZ) is located at the convergence of the Sunda, Australia, and Philippine Sea plates and only about 500 km long (Figure 1a). Magnetic anomalies and plate reconstruction indicate that the spreading of the Celebes Sea basin occurred along a north-northwest to south-southeast axis between approximately 48 and 40 Ma (Gaina and Müller, 2007; Hall, 2012; Rangin and Silver, 1991; Weissel, 1980). The southward subduction of the Celebes Sea plate began in approximately 9–5 Ma (Hall, 2012; Lai et al., 2021). The maximum depth of the subducted plate is about 260 km (Figure 1b). It has been overlooked as an excellent location for the study of the transition from passive to active margin (Hall, 2019).

Trench migration is closely correlated with overriding plate deformation and lateral migration of the subducted slab (Funicello et al., 2008; Holt et al., 2015; Schellart, 2008). The North Sulawesi Trench has retreated since the post-Miocene. Now, the overriding plate–North Arm of Sulawesi is rotating clockwise around its eastern end (Socquet et al., 2006) (Figure 1a). The conventional view is that the collision of the surrounding plates led to the formation of the NSSZ and the retreat of the trench (Kopp et al., 1999; Silver et al., 1983). However, the Sunda plate is moving slowly towards the southeast, while the Australia plate (in the south) and the Philippine Sea plate (in the northeast) are moving rapidly towards the northeast and the northwest, respectively (Figure 1a). If the movement of these three plates was the dominant mechanism underlying the retreat of the North Sulawesi Trench, the North Arm of Sulawesi would have been more prone to counterclockwise. Thus, the trench retreat and rotation mechanism of the North Sulawesi Trench remains unclear.

In this study, we conduct a series of thermomechanical model simulations to investigate the initial subduction and trench retreat mechanisms of the NSSZ, which is representative of the transition of a passive margin into a subduction zone. Variable boundary conditions are applied, representing different dynamic

mechanism. Trench retreat is driven by either overriding plate or subducted plate, which results in different regime diagrams. The model results are compared to the observations in North Sulawesi. The mechanism of model that best fit the observations is the subduction and trench movement mechanism of the NSSZ.

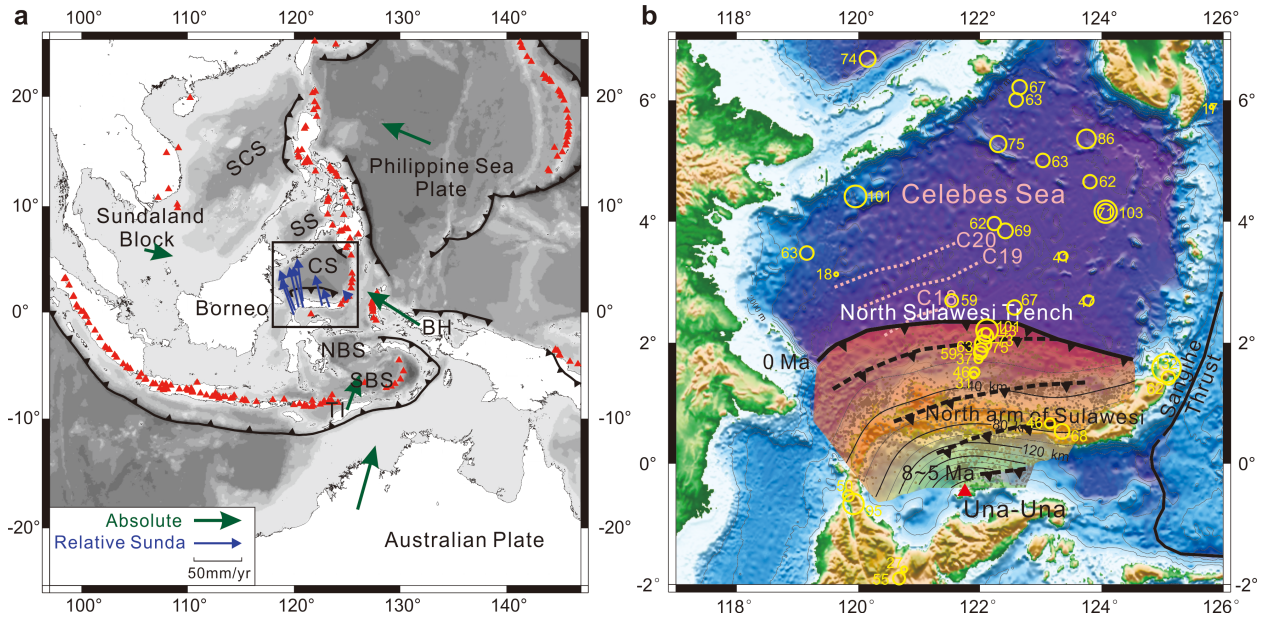


**Figure 1.** Structure-tectonic maps of the Celebes Sea and surrounding area. (a) Location of the study area—Celebes Sea (CS)—within the wider Southeast Asian region, including the Sulu Sea (SS), the South China Sea (SCS), the north Banda Sea (NBS) and the south Banda Sea (SBS). Thick lines indicate subduction zones; triangles on the lines indicate the down-dip direction. Plate motions are indicated by the arrows (Mustafar et al., 2017; Kreemer et al., 2014). Red triangles indicate volcanoes (Global Volcanism Program, 2013). (b) Regional topographic map. The yellow hollow circles are heat flow measurements (Fuchs et al., 2021). The pink dashed lines show the major magnetic anomalies (Weissel, 1980). The irregular shape with transparent colour gradient represents the subducted plate; colours indicate depth. The dotted lines with triangles indicate trench retreat. Events in the EHB catalogue (Engdahl et al., 2020) are represented by black circles.

### 1. Model setup

We used the geodynamic code ASPECT (Advanced Solver for Problems in Earth’s ConvecTion, version 2.3.0-pre) to setup a series of 2D subduction models. The initial model consists of oceanic plate and continental plate on either side (Figure 2a). According to the evolutionary history of NSSZ, the age of oceanic plate is taken to be 40 Ma. The oceanic lithosphere geotherm corresponds to a

half-space cooling model for a seafloor age of 40 Ma. The thickness of oceanic plate is therefore set to 82 km. The oceanic crust consists of two layers and is 10 km thick in total. The composition for the mantle part of the oceanic lithosphere and for the asthenosphere are taken to be identical. The density of them is both set to  $3300 \text{ kg/m}^3$ . The continental plate consists of upper crust, lower crust and lithospheric mantle. The continental crust is set to 30 km based on the current crustal thickness of Sulawesi (Fauzi et al., 2021). Because the initial lithospheric thickness, density of lithospheric mantle and ocean-continent transition angle have never been definitely settled, we vary the values of these three parameters to investigate their effect on the spontaneous subduction (Table 1). Temperature structure of the continental plate is controlled by the lithospheric thickness and is defined by a steady state profile from  $0 \text{ }^\circ\text{C}$  at the surface to  $1300^\circ\text{C}$  at the base of lithosphere (Figure 2a).

Spontaneous and induced subductions are modelled by controlling the boundary conditions and density differences between oceanic plate and asthenosphere. The spontaneous models (Experiment 1~24) have all free slip boundaries (Figure 2a) and the Gabbro-Eclogite phase transition for the oceanic crust was implemented. Density of oceanic crust increases from  $3000 \text{ kg/m}^3$  to  $3450 \text{ kg/m}^3$  at pressures of  $\sim 1.9 \text{ GPa}$  ( $\sim 60 \text{ km}$  depth). In the induced model (Experiment 25~30), horizontal far field forces are represented by specifying a convergence velocity ( $V_{\text{in}}$ ) on one side of the overriding plate; the Gabbro-Eclogite phase transition for the oceanic crust was not executed.

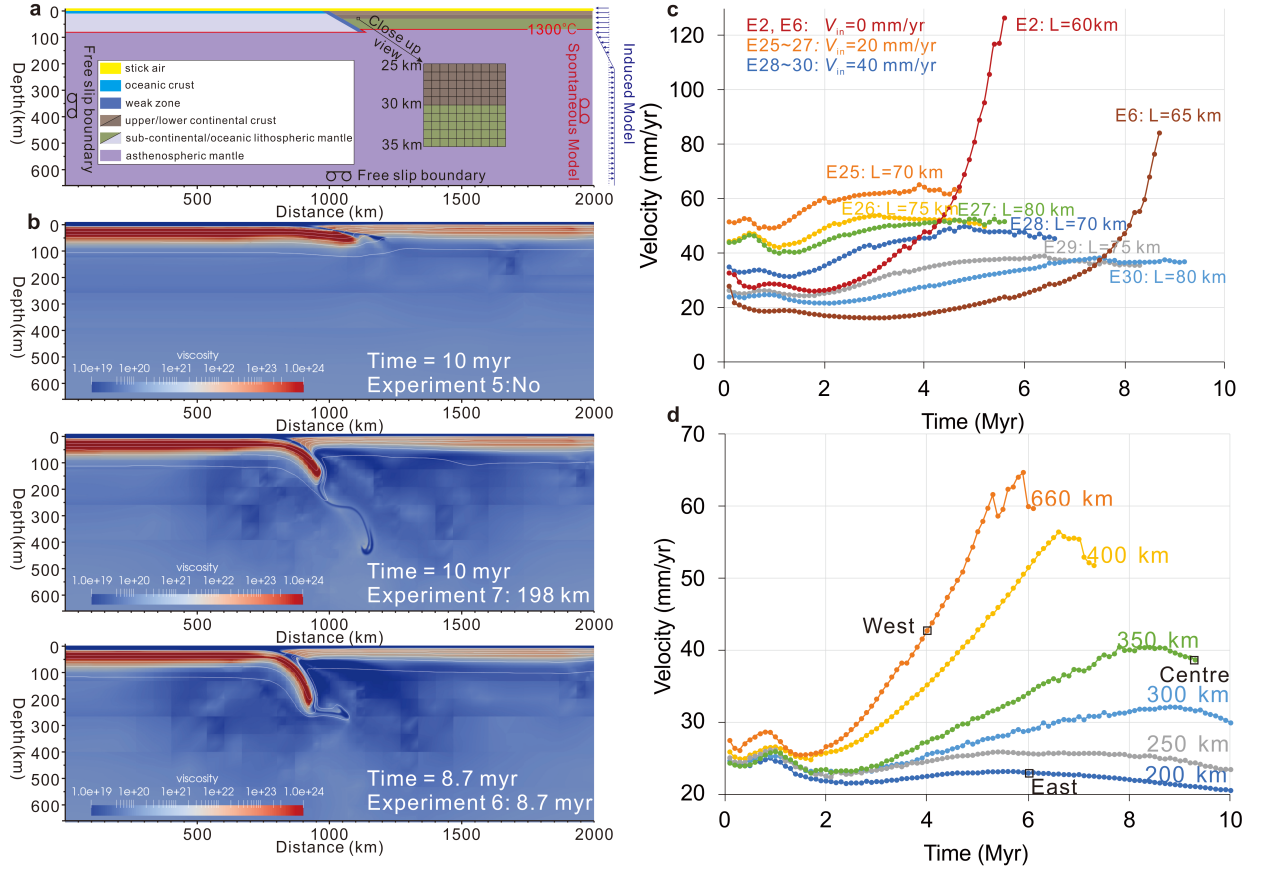


**Figure 2.** Initial model and modeling results. (a) Initial model setup with model geometry, layer characteristics, and thermal configuration. (b) Three cases show different results: no subduction (Experiment 5); subducted slab did not reach a depth of 260 km within 10 myr (Experiment 7); subduction depth of 260 km within 10 myr (Experiment 6). (c) Variation of trench retreat velocities with time for experiments with different mechanism (Density of continental lithospheric mantle = 3275 kg/m<sup>3</sup>; Ocean-continent transition angle = 30°). (d) Trench retreat velocity of the coupled model with depth 660 km, 400 km, 350 km, 300 km, 250 km, 200 km. West, Centre, East indicate the trench retreat velocity on the western side, centre and eastern side of Celebes Sea, respectively.

**Table 1.** Parameters and Descriptions of Numerical Experiments

Experiment	$V_{in}$ (mm/yr)	Thickness of continental plate (km)	Density of Continental lithospheric mantle
1	0	60	3275
2	0	60	3275
3	0	60	3275

Experiment	$V_{in}$ (mm/yr)	Thickness of continental plate (km)	Density of Continental lithospheric mantle
4	0	60	3275
5	0	65	3275
6	0	65	3275
7	0	65	3275
8	0	65	3275
9	0	70	3275
10	0	70	3275
11	0	70	3275
12	0	70	3275
13	0	60	3250
14	0	60	3250
15	0	60	3250
16	0	60	3250
17	0	65	3250
18	0	65	3250
19	0	65	3250
20	0	65	3250
21	0	70	3250
22	0	70	3250
23	0	70	3250
24	0	70	3250
25	40	70	3275
26	40	75	3275
27	40	80	3275
28	20	70	3275
29	20	75	3275
30	20	80	3275
31	20	75	3275
32	20	75	3275
33	20	75	3275
34	20	75	3275
35	20	75	3275
36	20	75	3275

### 3 Model Results

#### 3.1 Parameters that affect spontaneous subduction

Since the subduction initiation of NSSZ occurred at 5–9 Ma and the maximum depth of the subducted slab is about 260 km at present. The simulation ends when the subducted slab reaches a depth of 260 km or the time reaches 10 myr. If the oceanic slab does not exceed a depth of 150 km within 10 myr, we denote it by “No” (Figur 2b and Table 1). If the maximum depth of the subducted slab

is deeper than 150 km but shallower than 260 km (Figure 2b), we list the depth. For the experiments where the slab reached 260 km depth within 10 myr, we list this time (Figure 2b).

Experiments show transition from fast to slow subduction with increasing thickness of the continental lithosphere. Spontaneous subduction initiation is almost impossible to occur with 70 km or more thick continental plate (Experiment 9–12, 21–24). The effect of density contrast is opposite to that of the thickness of the continental plate. A larger density contrast promotes spontaneous subduction initiation. The ocean-continent boundary angle has a nonlinear effect on the spontaneous subduction initiation. Either too large ( $60^\circ$ ) or too small ( $15^\circ$ ) angle are all adverse to spontaneous subduction initiation. The thickness and density of the continental lithospheric mantle and the ocean-continent boundary angle all affect whether subduction initiation occurs spontaneously. It suggests that the force due to the density difference between the continental and oceanic plate is the main force leading to the spontaneous subduction initiation.

### 3.2 Trench retreat velocity in spontaneous and induced model experiments

Trench location and speed are inferred from the location and speed of the edge of the continental crust that is the farthest forward in the model. In all spontaneous and induced model experiments, trench retreat speed increases and then decreases during the first 1–2 myr (Figure 2c). At the beginning of the simulation period, the density difference between the continental and oceanic crusts gives rise to lateral stresses that push the continental crust towards the ocean; as the difference between the stresses decreases, trench retreat speed decreases gradually. This process is active in approximately 2 myr.

After the first 2 myr in the spontaneous model (Figure 2c), subduction depth increases, the trench retreat velocity increases correspondingly. The increasing begins slowly, then more and more rapidly. It is because as the oceanic plate sinks, there are more and more eclogite-face oceanic crust to increase the negative buoyancy of the subducted slab. In the induced model, the trench retreat speed increasing slowly, then becoming almost constant. The final speed is slightly greater than the specified velocity  $V_{in}$ .

### 3.3 Deformation and heat flow of the overriding plate

The deformation of the overriding plate varies in the different subduction models. In the spontaneous subduction model, the rollback of the subducted plate obviously causes stretching of the overriding plate. The crustal thickness decreased from 30 km to about 23 km (eg. Experiment 2, 3). In the induced subduction model, the overriding plate thrusts over the subducted plate, and the overriding plate is slightly thinned (Experiment 25–30). The latest published geological profile of the North Arm of Sulawesi indicates lithospheric significant extension between the Late Miocene and Pliocene (Nugraha et al., 2022, Advokaat et al., 2017), which is consistent with the results of the spontaneous subduction model.

The heat flow of the overriding plate is closely related to the lithospheric thick-

ness either in spontaneous or induced model experiments. It is opposite to the continental lithospheric thickness. The values of heat flow listed in Table 1 is the calculated surface heat flow which lies at a distance of 100 km above the top of the subducted slab. It corresponds to the location of the maximum heat flow ( $68 \text{ mW/m}^2$ ) on the North Arm of Sulawesi (Figure 1b). In all the experiments, the model with 75 km thick continental lithosphere has the closest value to that observation. The heat flow values in models have a 70 km or thinner lithosphere are all greater than the maximum observed values.

## 4 Discussion

### 4.1 Implications for transition of passive margins into subduction zones

The mechanism of subduction initiation at passive margins have been studied by several numerical simulations (Faccenna et al., 1999; Goren et al., 2008; Marques et al., 2014; Turcotte et al., 1977; Zhou et al., 2020). Our intention is not repeat other studies and prove the feasibility of spontaneous subduction initiation at passive margins, but to estimate the subduction mechanism through the constraints of the geological case—NSSZ. The spontaneous and induced subduction models represent the extreme cases of subduction driven by horizontal far-field forces and of subduction driven by the negative buoyancy of the down-going plate itself. Examples of completely spontaneous or induced mechanisms are difficult to reproduce the evolution of NSSZ—subduction depth of 260 km after approximately 5–9 myr,  $68 \text{ mW/m}^2$  heat flow of the overriding plate and obvious extended continental crust. Because the mainly force that cause the oceanic plate to bend and sink in spontaneous subduction initiation is lateral stress, which is caused by the density difference between the continental plate and the oceanic plate (Nikolaeva et al., 2010). A thick crust and hot lithosphere are necessary to produce the sufficiently large lateral stress (Nikolaeva et al., 2010). According to the present crustal structure and heat flow of North Arm of Sulawesi, spontaneous subduction initiation is unlike to occur in the NSSZ. Therefore, an external force is necessary to push the continental plate towards the oceanic plate in the early stage of subduction initiation. For the NSSZ, the external force may originate mainly from the collision of the surrounding plates. Because since the Cenozoic, Sulawesi has been at the center of the convergence of surrounding plates (Hall, 2012). This induced mechanism dominates the early stage of subduction initiation, which takes about 2 myr. Once the oceanic crust reaches the depths of  $\sim 60$  km where eclogite transformation can occur, the main force controlling the subduction begin to change from the horizontal external force to the vertical negative buoyancy of the subducted slab. The subsequent subduction, trench retreat and extension of continental crust are all mainly depend on the negative buoyancy of the subducted slab, as exhibitions in spontaneous model experiments (Table 1 and Figure 2). In addition, adjacent areas in the same tectonic setting can also provide insight into the subduction process.

The Sula Deep, Tolo Trough and Cotobato Trench located near the North Sulawesi Trench (Figure 3a, d) are considered to examples of three stages in the

subduction initiation. Sula Deep and Tolo Trough is suggested to record the earliest stages and second stage in subduction development, respectively (Hall, 2019). Cotobato Trench is interpreted as the third stage where a seismically defined slab can be recognized (Hall, 2019). The North Sulawesi Trench represents the final stage, which indicates that subduction initiation is end and a mature subduction zone has been formed. From the topography of these trenches (Figure 3), we can see that each trench has a different landward slope. The areas (Sula Deep and Tolo Trough) in early stage of subduction initiation, has a very steep landward slope (Figure 3b, c). As the subduction development (Cotobato Trench and North Sulawesi Trench), the landward slope changes from steep to gentle (Figure 3e, f).

There are obvious differences in landward slope angles vary in different mechanisms models. In the spontaneous numerical model, the slope gradually smooth with the subduction development (Figure 3g). While the slope in induced model is steeper than that in spontaneous model and the slope can be maintained at a steeper state under the push of far field forces (Figure 3h). Combining the steeper slope in the Sula Deep and Tolo Trough and gentle slope in Cotobato Trench and North Sulawesi Trench, we could also suggest the subduction slab controlled the retreat of the trench.

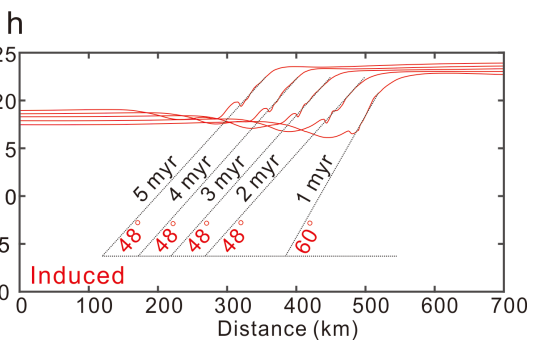
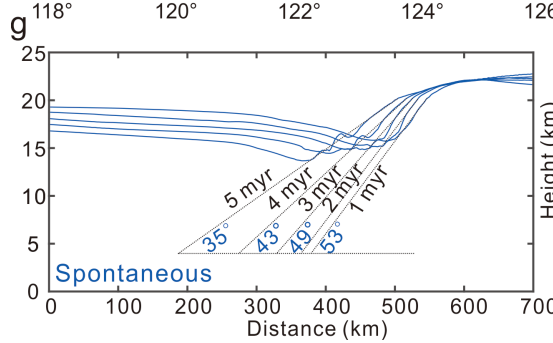
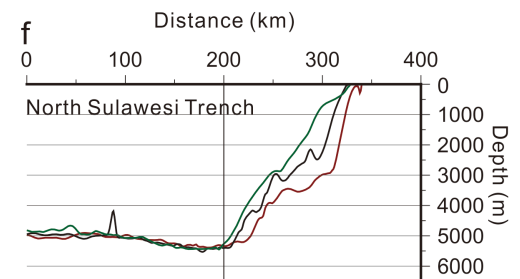
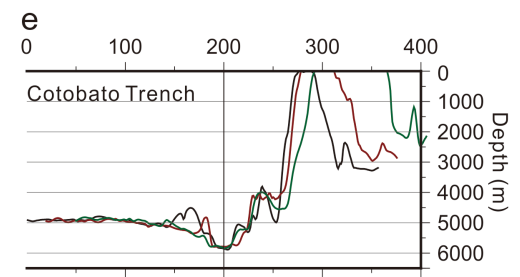
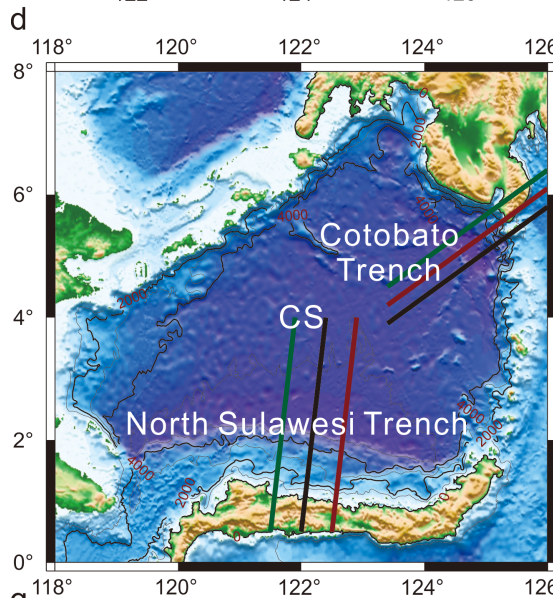
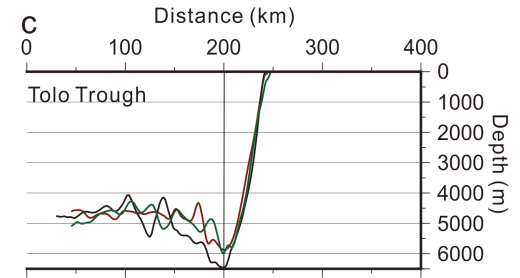
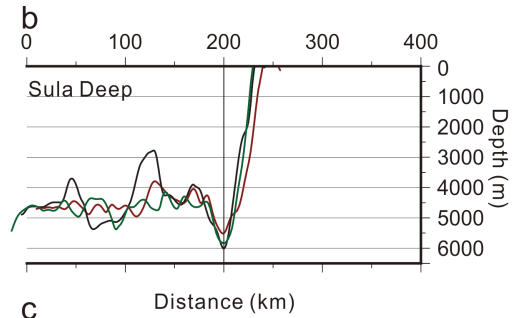
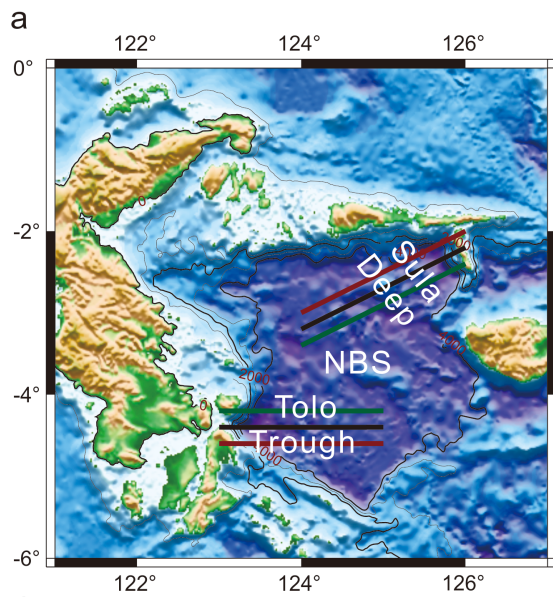


**Figure 3.** The topography profiles of the Sula Deep (b), Tolo Trough (c), Cotobato Trench (e), and North Sulawesi trench (f) and the topographic results simulated by the spontaneous model (g) and induced model (h). Location of Celebes Sea (CS) and north Banda Sea (NBS) are shown in Figure 1a. The black vertical lines at 200 km in (b), (c), (e), (f) indicate the trench location. We put the deepest position of every topography profiles at this location. Because the proportion of horizontal axis and vertical axis is not practical, the angles in the figures (g) and (h) are only used to compare with each other, not the true angles.

#### 4.2 Rotation of the North Arm of Sulawesi

The clockwise rotation of the North Arm of Sulawesi is also consistent with the spontaneous retreat of the North Sulawesi Trench. The negative buoyancy drags the slab down and promotes mantle flow, which determines trench retreat and deformation of the overriding plate (Alsaif et al., 2020). Seismic tomography shows that the Sangihe slab is subducting westward below the Celebes Sea plate (Hall and Spakman, 2015; Hayes et al., 2018). The subduction depth of the Sangihe slab increases from east to west; hence, the distance between the Celebes Sea plate and the Sangihe slab decreases from west to east, and the two plates are in contact on the eastern side of the Celebes Sea plate (Figure S1). Therefore, the Sangihe slab substantially reduces the space that is available for subduction on the eastern side of the Celebes Sea plate.

This is a complex 3-D situation, we can first simplify it to a two-dimensional model to simulate it. If we cut a section along the north-south direction (Figure S1). The Sangihe slab will be shown as a rectangular block below Celebes Sea on the profile. The distance between the top of the Sangihe slab and the earth’s surface on the west side is larger than that on the east side. So we can take the top of the Sangihe slab as the bottom of the model to build simplified models. We conduct experiments using the spontaneous subduction model; model depth is reduced from 660km to 400 km, 350 km, 300 km, 250 km and 200 km, respectively, while parameters and boundary conditions are held constant. We find that the reduction of the space available for subduction leads to the decrease of mantle convection velocity, which in turn reduces the trench retreat velocity (Figure 2d). These results are consistent with the hypothesis that the Sangihe slab reduces the space that is available for subduction, inhibiting spontaneous subduction and slowing down trench retreat on the eastern side (at about 123.5°E) of the Celebes Sea (“East” in Figure 2d). Although the length of the subducted slab is larger on the centre (at about 122°E) than the western side (at about 120.5°E) of Celebes Sea, there is always plenty of space for subduction on the western side of the Celebes Sea. As marked by “West” in Figure 2d, the slab reached to a depth of 150 km and the trench retreat speed increased to ~43 mm/yr during a short time. By contrast, space for subduction on the centre is always limited. As marked by “Centre” in Figure 2d, the trench retreat speed is only ~37 mm/yr, although its subducted slab has reached a depth of 260 km. Hence, trench retreat speed decreases from the western side

to the eastern side of the Celebes Sea, resulting in the clockwise rotation of the North Arm of Sulawesi.

However, the 2D models ignored the effect of toroidal flow around the slab edge. Hence, we build a 3D model to simulate this complex natural 3D system (Figure 4). The 3D model consists of a continental plate as overriding plate and two oceanic subducted plates. The subduction direction of the two subduction plates is orthogonal. Model parameters and rheology are same with the 2D model. As we can see from the simulation result (Figure 4), the trench retreat speed simulated by 3D model is also roughly equal to the velocity of the North Arm of Sulawesi measured by GPS. According to the modelling results, we found that the subduction-driven mantle wedge flow is much faster than the toroidal flow around the slab edge. The mantle wedge flow of Sangihe slab is mainly parallel to the North Sulawesi Trench which has little effect on the subduction of Celebes Sea slab. The most important factor that affecting the subduct rate of Celebes Sea slab is also the available space for subduction. Therefore, we proposed that the reason for the clockwise rotation of the North Arm of Sulawesi at present is the presence of the Sangihe slab.

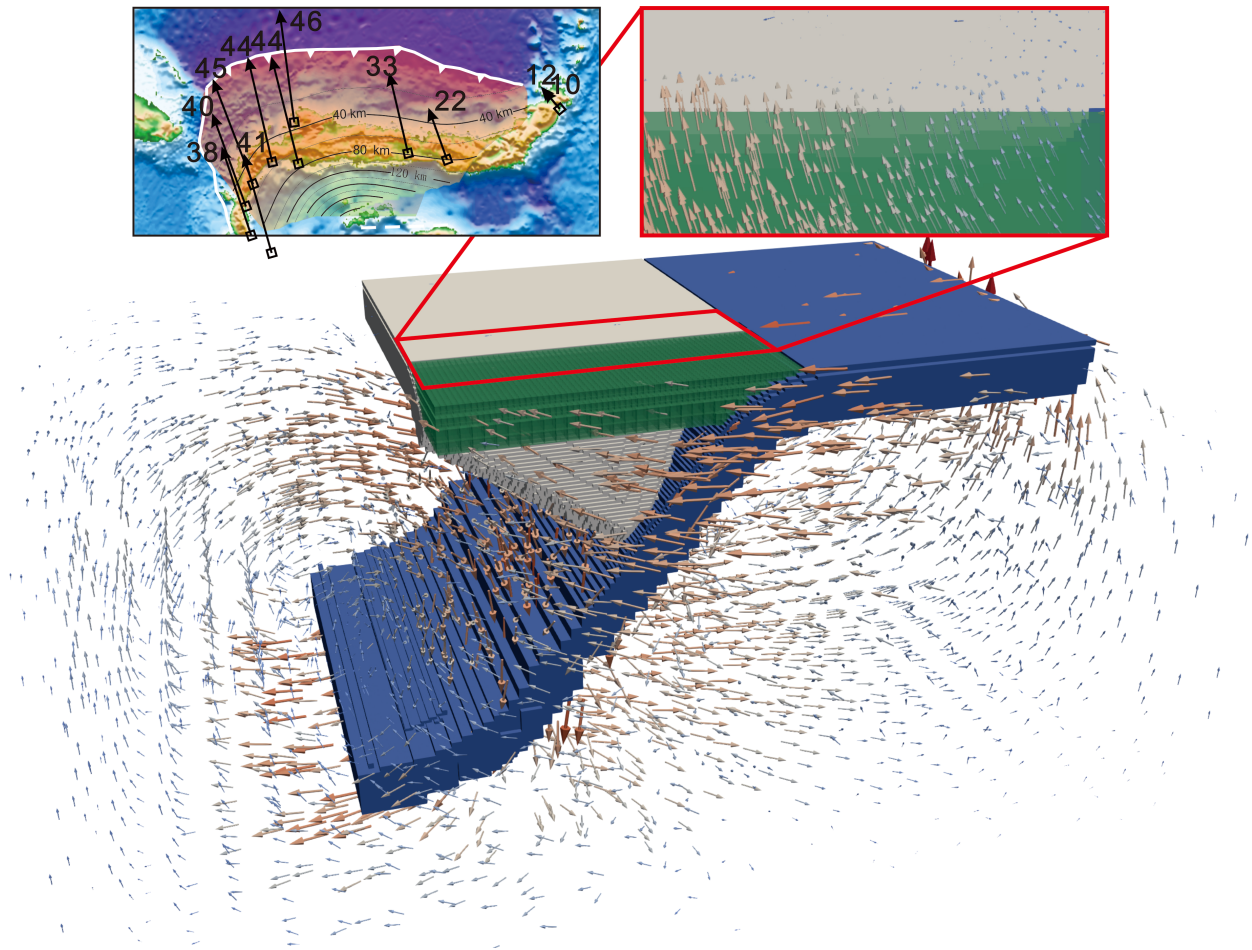


**Figure 4.** 3D Schematic model (view to the northwest) of the North Sulawesi Subduction Zone. The gray plate represents the Celebes Sea plate. The blue slab represents the Sangihe slab. Arrows indicate velocity. GPS velocities of North Arm of Sulawesi are from Socquet et al. (2006)

## 5 Conclusions

The main conclusions we may draw from this study include the following:

1. Our numerical experiments demonstrate the crucial role that the buoyancy of the down-going plate itself plays in trench retreat as a passive margin transitions into an active margin, even though the initial stage is dominated by the external force.
2. The Sangihe slab reduces the space that is available for subduction, inhibiting spontaneous subduction and slowing down trench retreat on the eastern side of the Celebes Sea, which well explains the clockwise rotation of the North Arm

of Sulawesi.

#### Acknowledgments

M. D., T. Y. H., and J. Z. acknowledge financial support from the National Natural Science Foundation of China (91858212, 41906056, and 42076068) and the International Partnership Program of the Bureau of International Cooperation of the Chinese Academy of Sciences (132A11KY5B20180020). CC. L. was supported by the Isaac Newton Trust in Cambridge and GCRF (G102642). The authors also thank the Computational Infrastructure for Geodynamics (geodynamics.org), which is funded by the NSF under awards EAR-0949446 and EAR-1550901, for supporting the development of ASPECT.

#### Data Availability Statement

The version of ASPECT is available at <https://doi.org/10.5281/zenodo.5131909>. All data that this numerical study is based on can be found in Table S1.

#### References

- Advokaat, E. L., Hall, R., White, L. T., Watkinson, I. M., Rudyawan, A., & BouDagher-Fadel, M. K. (2017). Miocene to recent extension in NW Sulawesi, Indonesia, *Journal of Asian Earth Sciences*, *147*, 378-401. <https://doi.org/10.1016/j.jseaes.2017.07.023>
- Alsaif, M., F. Garel, F. Gueydan, & D. R. Davies (2020). Upper plate deformation and trench retreat modulated by subduction-driven shallow asthenospheric flows. *Earth and Planetary Science Letters*, *532*, <https://doi.org/10.1016/j.epsl.2019.116013>
- Bangerth, W., Dannberg, J., Gassmoeller, R., & Heister, T. 2020. ASPECT v2.2.0. (version v2.2.0). Zenodo. <https://doi.org/10.5281/ZENODO.3924604>
- Engdahl, E. R., Di Giacomo, D., Sakarya, B., Gkarlaoui, C. G., Harris, J., & Storchak, D. A. (2020). ISC-EHB1964-2016, an improved data set for studies of Earth structure and global seismicity. *Earth and Space Science*, *7*, e2019EA000897. <https://doi.org/10.1029/2019EA000897>
- Faccenna, C., Giardini, D., Davy, P., & Argentieri, A. (1999). Initiation of subduction at Atlantic-type margins: Insights from laboratory experiments. *Journal of Geophysical Research*, *104*, 2749-2766. <https://doi.org/10.1029/1998JB900072>
- Fauzi M. F., Anggraini, A., Riyanto, A., Ngadmanto, D., Suryanto, W., 2021. Crustal thickness estimation in Indonesia using receiver function method, IOP Conf. Series: Earth and Environmental Science 873 (2021) 012086. <https://doi.org/10.1088/1755-1315/873/1/012086>.
- Fuchs, Sven; Norden, Ben; International Heat Flow Commission (2021): The Global Heat Flow Database: Release 2021. GFZ Data Services. <https://doi.org/10.5880/figeo.2021.014>

- Funiciello, F., C. Faccenna, A. Heuret, S. Lallemand, E. Di Giuseppe, & T. W. Becker (2008). Trench migration, net rotation and slab–mantle coupling. *Earth and Planetary Science Letters*, 271(1-4), 233-240. <https://doi.org/doi:10.1016/j.epsl.2008.04.006>
- Gaina, C., & Müller, D. (2007). Cenozoic tectonic and depth/age evolution of the Indonesian gateway and associated back-arc basins, *Earth-Science Reviews*, 83(3-4), 177-203. <https://doi.org/10.1016/j.earscirev.2007.04.004>
- Glerum, A., Thieulot, C., Fraters, M., Blom, C., & Spakman, W. (2018). Non-linear viscoplasticity in ASPECT: benchmarking and applications to subduction, *Solid Earth*, 9(2), 267-294. <https://doi.org/10.5194/se-9-267-2018>
- Global Volcanism Program, 2013. Volcanoes of the World, v. 4.9.4 (17 Mar 2021). Venzke, E (ed.). Smithsonian Institution. Downloaded 23 Apr 2021. <https://doi.org/10.5479/si.GVP.VOTW4-2013>.
- Goren, L., Aharonov, E., Mulugeta, G., Koyi, H. A., & Mart, Y. (2008). Ductile deformation of passive margins: A new mechanism for subduction initiation, *Journal of Geophysical Research: Solid Earth*, 113(B8). <https://doi.org/10.1029/2005jb004179>
- Hall, C. E., Gurnis, M., Sdrolias, M., Lavier, L. L., Müller, R. D. (2003). Catastrophic initiation of subduction following forced convergence across fracture zones. *Earth and Planetary Science Letters*, 212, 15-30. [https://doi.org/10.1016/S0012-821X\(03\)00242-5](https://doi.org/10.1016/S0012-821X(03)00242-5)
- Hall, R. & Spakman, W. (2015). Mantle structure and tectonic history of SE Asia. *Tectonophysics* 658, 14-45. <https://doi.org/10.1016/j.tecto.2015.07.003>
- Hall, R. (2012). Late Jurassic–Cenozoic reconstructions of the Indonesian region and the Indian Ocean, *Tectonophysics*, 570-571, 1-41. <https://doi.org/10.1016/j.tecto.2012.04.021>
- Hall, R. (2019). The subduction initiation stage of the Wilson cycle, *Geological Society, London, Special Publications*, 470(1), 415-437. <https://doi.org/10.1144/SP470.3>
- Hayes, G. P., Moore, G. L., Portner, D. E., Hearne, M., Flamme, H., Furtney, M., & Smoczyk, G. M. (2018). Slab2, a comprehensive subduction zone geometry model, *Science*, 362(6410), 58-61. <https://doi.org/10.1126/science.aat4723>
- Heister, T., Dannberg, J., Gassmöller, R., & Bangerth, W. (2017). High Accuracy Mantle Convection Simulation through Modern Numerical Methods-II: Realistic Models and Problem. *Geophysical Journal International*, 210, 833-851. <https://doi.org/10.1093/gji/ggx195>
- Hirth, G. & Kohlstedt, D. Rheology of the upper mantle and the mantle wedge: a view from the experimentalists. in *Inside the Subduction Factory* (ed. Eiler, J.) Vol. 183 of Geophysical Monograph (American Geophysical Union, 2003).

- Holt, A. F., Becker, T. W., & Buffett, B. A. (2015). Trench migration and overriding plate stress in dynamic subduction models. *Geophysical Journal International*, 201, 172-192. <https://doi.org/10.1093/gji/ggv011>
- Hu, J., & Gurnis, M. (2020). Subduction Duration and Slab Dip. *Geochemistry, Geophysics, Geosystems*, 21, e2019GC008862. <https://doi.org/10.1029/2019GC008862>
- Kopp, C., Flueh, E. R., & Neben, S. (1999). Rupture and accretion of the Celebes Sea crust related to the North Sulawesi subduction combined interpretation of reflection and refraction seismic measurements. *Journal of Geodynamics*, 27(3), 309-325. [https://doi.org/10.1016/S0264-3707\(98\)00004-0](https://doi.org/10.1016/S0264-3707(98)00004-0)
- Kreemer, C., Blewitt, G., & Klein, E. C. (2014). A geodetic plate motion and Global Strain Rate Model. *Geochemistry, Geophysics, Geosystems*, 15, 3849-3889. <https://doi.org/10.1002/2014GC005407>
- Kronbichler, M., Heister, T., & Bangerth, W. (2012). High Accuracy Mantle Convection Simulation through Modern Numerical Methods. *Geophysical Journal International*, 191, 12-29. <https://doi.org/10.1111/j.1365-246X.2012.05609.x>
- Lai, C.-K., Xia, X.-P., Hall, R., Meffre, S., Tsikouras, B., Rosana Balangué-Tarriela, M. I., et al. (2021). Cenozoic evolution of the Sulu Sea arc-basin system: An overview. *Tectonics*, 40, e2020TC006630. <https://doi.org/10.1029/2020TC006630>
- Lallemand, S., Heuret, A., & Boutelier, D. (2005). On the relationships between slab dip, back-arc stress, upper plate absolute motion, and crustal nature in subduction zones. *Geochemistry, Geophysics, Geosystems*, 6, Q09006. <https://doi.org/10.1029/2005GC000917>
- Leng, W., & Gurnis, M. (2015). Subduction initiation at relic arcs. *Geophysical Research Letters*, 42(17), 7014-7021. <https://doi.org/10.1002/2015gl064985>
- Marques, F. O., Nikolaeva, K., Assumpção, M., Gerya, T. V., Bezerra, F. H. R., do Nascimento, A. F., & Ferreira, J. M. (2013). Testing the influence of far-field topographic forcing on subduction initiation at a passive margin. *Tectonophysics*, 608, 517-524. <https://doi.org/10.1016/j.tecto.2013.08.035>
- Marques, F. O., Cabral, F. R., Gerya, T. V., Zhu, G., & May, D. A. (2014). Subduction initiates at straight passive margins. *Geology*, 42, 331-334. <https://doi.org/10.1130/G35246.1>
- Mueller, S., & Phillips, R. J. (1991). On The initiation of subduction, *Journal of Geophysical Research*, 96(B1), 651-665. <https://doi.org/10.1029/90jb02237>
- Mustafar, M. A., Simons, W. J. F., Tongkul, F., Satirapod, C., Omar, K. M., & Visser, P. N. A. M. (2017). Quantifying deformation in North Borneo with GPS. *Journal of Geodesy*, 91, 1241-1259. <https://doi.org/10.1007/s00190-017-1024-z>

- Nikolaeva, K., Gerya, T. V., Marques, F. O. (2010). Subduction initiation at passive margins: Numerical modeling. *Journal of Geophysical Research*, *115*, B03406. <https://doi.org/10.1029/2009JB006549>
- Nikolaeva, K., Gerya, T. V., Marques, F. O. (2011). Numerical analysis of subduction initiation risk along the Atlantic American passive margins. *Geology* *39*, 463-466. <https://doi.org/10.1130/G31972.1>
- Nugraha, A. M. S., Hall, R., & BouDagher-Fadel, M. (2022). The Celebes Molasse: A revised Neogene stratigraphy for Sulawesi, Indonesia. *Journal of Asian Earth Sciences*, *228*, 105140. <https://doi.org/10.1016/j.jseaes.2022.105140>
- Rangin, C., & Silver, E. A. (1991). Neogene tectonic evolution of the Celebes-Sulu basins: new insights from leg 124 drilling. *Proceeding of the Ocean Drilling Program, Scientific Result*, *124*, 51-63.
- Rey, P., Coltice, N. & Flament, N. (2014). Spreading continents kick-started plate tectonics. *Nature*, *513*, 405–408. <https://doi.org/10.1038/nature13728>
- Rutter, E. H. & Brodie, K. H. (2004). Experimental grain size-sensitive flow of hotpressed Brazilian quartz aggregates. *Journal of Structural Geology*, *26*, 2011–2023. <https://doi.org/10.1016/j.jsg.2004.04.006>
- Rybacki, E., Gottschalk, M., Wirth, R. & Dresen, G. (2006). Influence of water fugacity and activation volume on the flow properties of fine-grained anorthite aggregates. *Journal of Geophysical Research: Solid Earth*, *111*, 3663. <https://doi.org/10.1029/2005JB003663>
- Schellart, W. P. (2008), Subduction zone trench migration: Slab driven or overriding-plate-driven? *Physics of the Earth and Planetary Interiors*, *170*(1-2), 73-88, <https://doi.org/10.1016/j.pepi.2008.07.040>
- Sharples, W., Jadamec, M. A., Moresi, L. N., & Capitanio, F. A. (2014). Overriding plate controls on subduction evolution, *Journal of Geophysical Research: Solid Earth*, *119*(8), 6684-6704. <https://doi.org/10.1002/2014jb011163>
- Silver, E. A., McCaffrey, R., & Smith, R. B. (1983). Collision, Rotation, and the Initiation of Subduction in the Evolution of Sulawesi, Indonesia. *Journal of Geophysical Research*, *88*, 9407-9418. <https://doi.org/10.1029/JB088iB11p09407>
- Socquet, A., Simons, W., Vigny, C., McCaffrey, R., Subarya, C., Sarsito, D., et al. (2006). Microblock rotations and fault coupling in SE Asia triple junction (Sulawesi, Indonesia) from GPS and earthquake slip vector data, *Journal of Geophysical Research*, *111*(B8). <https://doi.org/10.1029/2005jb003963>
- Stern, R. J. (2004). Subduction initiation: spontaneous and induced, *Earth and Planetary Science Letters*, *226*(3-4), 275-292. [https://doi.org/10.1016/s0012-821x\(04\)00498-4](https://doi.org/10.1016/s0012-821x(04)00498-4)

- Stern, R. J., & Gerya, T. (2018). Subduction initiation in nature and models: A review, *Tectonophysics*, *746*, 173-198. <https://doi.org/10.1016/j.tecto.2017.10.014>
- Turcotte, D. L., Ahern, J. L. & Bird, J. M. (1977). The state of stress at continental margins. *Tectonophysics*, *42*, 1-28. [https://doi.org/10.1016/0040-1951\(77\)90014-2](https://doi.org/10.1016/0040-1951(77)90014-2)
- Turcotte, D. L., & Schubert, G. (2014). Geodynamics. Cambridge, UK: Cambridge University Press.
- Weissel, J.K. 1980. Evidence for Eocene oceanic crust in the Celebes Basin. In: Hayes, D.E. (Ed.), The Tectonic and Geologic Evolution of Southeast Asian Seas and Islands. American Geophysical Union, Geophysical Monograph Series, *23*, 37-47.
- Zhang, J., Hao, T., Dong, M., Xu, Y., Wang, B., Ai, Y., & Fang, G. (2021). Investigation of geothermal structure of the Sulawesi, using gravity and magnetic method. *Science China Earth Sciences*, *64*, 278-293. <https://doi.org/10.1007/s11430-020-9659-3>
- Zhong, X., & Li, Z. H. (2019). Forced Subduction Initiation at Passive Continental Margins: Velocity-Driven Versus Stress-Driven, *Geophysical Research Letters*, *46*(20), 11054-11064. <https://doi.org/10.1029/2019gl084022>
- Zhou, X., Li, Z. H., Gerya, T. V. & Stern, R. J. (2020). Lateral propagation-induced subduction initiation at passive continental margins controlled by pre-existing lithospheric weakness. *Science Advances*, *6*, eaaz1048. <https://doi.org/10.1126/sciadv.aaz1048>

*Geophysical Research Letters*

Supporting Information for

**Downgoing plate-buoyancy driven retreat of North Sulawesi Trench: transition of a  
passive margin into a subduction zone**

Miao Dong<sup>1,2\*</sup>, Tianyao Hao<sup>1, 2\*</sup>, Chuanchuan Lü<sup>3</sup>, Jian Zhang<sup>2</sup>

1 Key Laboratory of Petroleum Resource Research, Institute of Geology and Geophysics, Chinese  
Academy of Sciences, Beijing, 100029

2 University of Chinese Academy of Sciences, Beijing, 100049

3 Bullard Labs, Department of Earth Sciences, University of Cambridge, Cambridge CB3 0EZ UK

**Contents of this file**

Text S1

Tables S1

Figures S1

## Introduction

Text S1 summarizes basic equations of the numerical simulations and initial model domain and thermal configurations.

Tables S1 list parameters used in the numerical simulations.

Figure S1 shows how to simplified the 3-D situation to 2-D model.

### Text S1.

We use the Advanced Solver for Problems in Earth's Convection (ASPECT)(Bangerth et al., 2020; Heister et al., 2017; Kronbichler et al., 2012), which is a highly scalable open-source code, to develop a 2D numerical geodynamic model. The model solves the momentum, mass conservation and heat conservation equations:

$$-\nabla \cdot 2\eta\dot{\varepsilon} + \nabla P = \rho g, \quad (1)$$

$$\nabla \cdot \mathbf{v} = 0, \quad (2)$$

$$\rho C_p \left( \frac{\partial T}{\partial t} + \mathbf{v} \cdot \nabla T \right) - k \nabla^2 T = H, \quad (3)$$

where  $\eta$  is the effective viscosity (see equations (4)–(6)),  $\dot{\varepsilon}$  is the deviatoric strain rate tensor, which is given by  $\frac{1}{2}(\nabla \mathbf{v} + (\nabla \mathbf{v})^T)$ ,  $P$  is the pressure,  $\rho$  is the density, which is defined as  $\rho = \rho_0 (1 - \alpha(T - T_0))$  with  $T_0$  being the reference temperature,  $g$  is the gravitational acceleration,  $\mathbf{v}$  is the velocity,  $C_p$  is the specific heat capacity,  $T$  is the temperature,  $t$  is time,  $k$  is the thermal conductivity, and  $H$  is the volumetric heat source term that includes radiogenic heat, shear heating, and adiabatic heating.

We use the Drucker–Prager yield criterion and a visco-plastic rheology (Glerum et al., 2018) with dislocation and diffusion creep, which are incorporated into ASPECT in 2D via the following equations:

$$\eta_{\text{comp}} = \left( \frac{1}{\eta_{\text{diff}}} + \frac{1}{\eta_{\text{disl}}} \right)^{-1}, \quad (4)$$

$$\eta_{\text{diff}} = \frac{1}{2} A^{-1} d^m \exp \left( \frac{E_{\text{diff}} + PV_{\text{diff}}}{RT} \right), \quad (5)$$

$$\eta_{\text{disl}} = \frac{1}{2} A^n \left( \dot{\varepsilon}_{\text{II}} \right)^{\frac{1-n}{n}} \exp \left( \frac{E_{\text{disl}} + PV_{\text{disl}}}{nRT} \right), \quad (6)$$

where  $\eta_{\text{comp}}$  is the composite viscosity,  $\eta_{\text{diff}}$  is the diffusion creep,  $\eta_{\text{disl}}$  is the dislocation creep,  $A$  is the pre-exponential factor,  $n$  and  $m$  are stress and grain size exponents,  $\dot{\varepsilon}_{\text{II}}$  is the second invariant of the strain rate tensor, which is defined as  $\dot{\varepsilon}_{\text{II}} = \left( 0.5 \dot{\varepsilon}_{ij} \dot{\varepsilon}_{ij} \right)^{0.5}$ ,  $E$  is the activation energy,  $V$  is the activation volume,  $R$  is the gas constant. These parameters are determined from the flow law experiments (Table S1).

Frictional-plastic deformation is responsible for faulting and follows a pressure-dependent Drucker–Prager yield criterion:

$$\sigma_{\text{yeild}} = C_0 \cos \varphi + P \sin \varphi, \quad (7)$$

$$\eta_{\text{Drucker-Prager}} = \begin{cases} \eta_{\text{comp}}, & 2\eta_{\text{comp}} \dot{\varepsilon}_{\text{II}} < \sigma_{\text{yeild}} \\ \frac{\sigma_{\text{yeild}}}{2\dot{\varepsilon}_{\text{II}}}, & 2\eta_{\text{comp}} \dot{\varepsilon}_{\text{II}} > \sigma_{\text{yeild}} \end{cases}, \quad (8)$$

where  $\sigma_{\text{yeild}}$  is the yield stress,  $C_0$  is the cohesion, and  $\varphi$  is the angle of internal friction.

The final effective viscosity,  $\eta_{\text{Drucker-Prager}}$ , is capped by minimum and maximum viscosities. Table S1 shows the parameters that we use.

The initial 2D model domain is 2,000 km by 670 km (Figure. 2a), with adaptive mesh refinement for finite elements with large gradients in the viscosity, temperature, and composition. The adaptive mesh refinement parameters in our reference model

produce a maximum level of refinement corresponding to 1-km-wide finite element dimensions (in the lithosphere layer) and a minimum level of refinement corresponding to 64-km finite elements (in the lowermost mantle).

An initial internal free surface is simulated with a layer of sticky air on the top of the model and is 10 km thick. The overriding plate is simulated as a continental plate with an upper continental crust, lower continental crust, and an underlying lithospheric mantle with thicknesses of 30, 35, 40, 45, and 50 km, respectively. The subducted plate incorporates oceanic crust, which is 10 km thick, and the oceanic lithosphere, which has a thickness that is determined by the half-space cooling model (Turcotte and Schubert, 2014). The model is initiated with a weak zone between the subducted and overriding plates, which represents the pre-existing subduction interface. The angle between subducted and overriding plates is set to 15°, 30°, 45° and 60°, respectively.

The thermal structure of the initial model is as follows: the oceanic lithosphere geotherm corresponds to a half-space cooling model for a seafloor age of 40 Ma, the continental lithosphere varies from 0 to 1300 °C, which is calculated by solving the steady state heat conduction equation. The temperature gradient in the asthenospheric mantle is about 0.5 °C/km, and the upper and lower thermal boundaries are fixed.

**Table S1.** Physical properties of materials used in the numerical experiments (Hirth and Kohlstedt, 2003; Rutter and Brodie, 2004; Rybacki et al., 2006). Density values of asthenosphere and continental lithospheric mantle ( $\rho$ ) are set according to the model.

Parameters	Units	Asthenosphere	Air	Upper continental crust	Lower continental crust	continental Lithospheric mantle	Upper Oceanic crust	Lower Oceanic crust	Weak zone
thermal conductivity	$\text{W}\cdot\text{m}^{-1}\cdot\text{K}^{-1}$	3.3	82.5	2.5	2.5	3.3	2.5	2.5	3.3
specific heat capacity	$\text{J}\cdot\text{kg}^{-1}\cdot\text{K}^{-1}$	1000	1000	1000	1000	1000	1000	1000	1000
Density	$\text{kg}\cdot\text{m}^{-3}$	3300	1	2700	2838	$\rho$	3000~3450	3000~3450	3300
Thermal expansivity	$\text{K}^{-1}$	$2\times 10^{-5}$	0	$2\times 10^{-5}$	$2\times 10^{-5}$	$2\times 10^{-5}$	$2\times 10^{-5}$	$2\times 10^{-5}$	$2\times 10^{-5}$
Rheological Flow	-	Dry olivine		Wet quartzite	Wet anorthite	Dry olivine	Gabbro	Gabbro	Wet olivine
pre-exponential factor	$\text{Pa}^{-n}\cdot\text{m}^{-p}\cdot\text{s}^{-1}$	$2.37\times 10^{-15}$	$1\times 10^{-50}$	$1\times 10^{-50}$	$1\times 10^{-50}$	$2.37\times 10^{-15}$	$1\times 10^{-50}$	$1\times 10^{-50}$	$1\times 10^{-50}$
		$6.52\times 10^{-16}$	$5\times 10^{-19}$	$8.57\times 10^{-28}$	$7.13\times 10^{-18}$	$6.52\times 10^{-16}$	$2.2553\times 10^{-17}$	$1.3725\times 10^{-25}$	$2.03\times 10^{-15}$
Stress exponents	-	1	1	1	1	1	1	1	1
		3.5	1	4.0	3	3.5	2.3	4.7	3.5
activation energy	$\text{J}\cdot\text{mol}^{-1}$	$375\times 10^3$	0	0	0	$375\times 10^3$	0	$335\times 10^3$	0
		$530\times 10^3$	0	$223\times 10^3$	$345\times 10^3$	$530\times 10^3$	$154\times 10^3$	$485\times 10^3$	$497\times 10^3$
activation volume	$\text{m}^3\cdot\text{mol}^{-1}$	$4\times 10^{-6}$	0	0	0	$4\times 10^{-6}$	0	$4\times 10^{-6}$	$4\times 10^{-6}$
		$13\times 10^{-6}$	0	0	0	$18\times 10^{-6}$	0	0	$18\times 10^{-6}$
grain size exponents	-	3	0	1	1	3	0	0	1

Figure S1. Slab2 model for Celebes Sea and Sangihe slab

